Supplementary Information (SI) for Organic Chemistry Frontiers.
This journal is © the Partner Organisations 2024

Supporting Information

for

Remote control supramolecular switch using ring-substituted *peri*-naphthoindigo derivative

*Indraneel Debnath, Tirupati Roy, and Kingsuk Mahata**

Department of Chemistry, Indian Institute of Technology Guwahati, Guwahati -781039, India.
Email: kingsuk@iitg.ac.in, Fax: (+91) 361-258-2349

Table of contents

1. Materials and Methods

Chemicals were purchased from Avra, Himedia, Spectrochem and Merck, and used without further purification. The alkyl bromide was purchased from Spectrochem. Copper Nitrate, trifluoroacetic acid were obtained from Merck. Solvents were obtained from Merck, Deuterated chloroform was obtained from Sigma-Aldrich ($CDCl_3$: 99.8 atom %). HPLC and UV grade solvents were obtained either from Spectrochem or from Merck. Silica gel for column chromatography (60-120 mesh), butylboronic acid, cesium carbonate and bispinacolatodiborane were procured from Spectrochem. Analytical thin layer chromatography (TLC) plate (silica gel 60 GF254) was purchased from Merck. All of the visual observations and reaction monitoring in chromatography were done under either 254 nm or 365 nm light. NMR measurements were carried out either on a Bruker AscendTM 400 MHz spectrometer or on a Bruker Avance III 600 MHz NMR spectrometer using the deuterated solvent as the lock and the residual solvent as the internal reference. The chemical shifts were reported in δ (ppm) relative to the residual protonated solvent peak of the deuterated solvent - $CDCl_3$ (99.8% : δ_H = 7.26 ppm), C_6D_6 (99.6% : δ_H = 7.15 ppm), . NMR measurements were carried out at 295 K. The following abbreviations were utilized to describe the peak patterns: s = singlet, d = doublet, t = triplet, q = quartet, dd = doublet of doublet, dt = doublet of triplet, m = multiplet and br = broad. The Numbering of the carbons atoms of the structures are for the assignments of NMR signal only, and not in accordance with the IUPAC nomenclature rules. Absorbance studies were performed on a Cary 100 and Cary 3500 UV-Vis spectrophotometer, and depending on the concentrations, samples were loaded in quartz UV-cuvettes having either 1 mm or 10 mm path length. Emission studies were conducted on a Horiba Fluoromax-Plus-C fluorimeter using a 10 mm quartz cuvette. Correction of spectra was done by the correction factor implemented in the software. HRMS data were recorded either with a Agilent QTOF ESI-MS HAB-273 mass spectrometer using electrospray ionization (ESI) mode. Infra-red (IR) spectra were collected on a diamond tipped Perkin-Elmer Spectrum Two FT-IR spectrometer and frequencies are presented in reciprocal centimeter (cm^{-1})

2. Synthesis

Synthesis BuPNI was accomplished as per the following scheme. Compound **1** was prepared following a reported procedure.[1]

Scheme S1. Synthetic scheme for BuPNI.

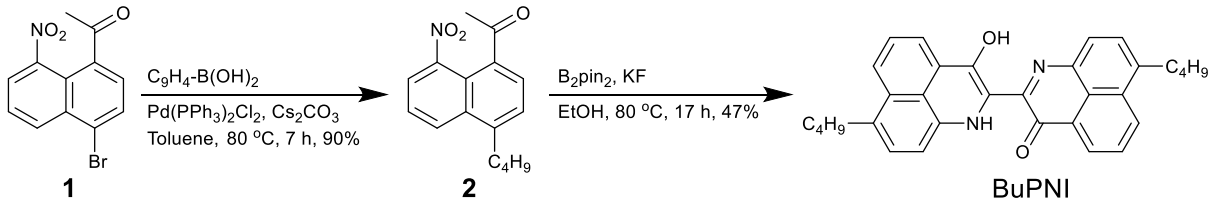

Synthesis of compound 2

To a solution of **1** (250 mg, 0.85 mmol) in toluene (10 mL), loaded in a Schlenk flask equipped with a stirring bar, butylboronic acid (104 mg, 1.02 mmol), $Pd(PPh_3)_2Cl_2$ (60 mg, 0.085 mmol) and Cs_2CO_3 (692 mg, 2.125 mmol) were added in quick succesion. The entire reaction system was purged with argon to maintain an inert atmosphere. The vessel was then dipped inside a pre-heated oil bath at 80 ℃ and the reaction mixture was stirred for 7 h at the same temperature. After cooling down to room temperature, toluene was evaporated under reduced reduced pressure. The residue was then dissolved in DCM, filtered, and evaporated to receive crude residue. The desired compound was received as yellow colored sticky solid after purification using column chromatography (SiO_2, EtOAc/hexane 1:9 v/v). Yield 208 mg, 91%. ^{1}H NMR (400 MHz, $CDCl_3$) δ = 8.34 (d, ^3J = 8.4 Hz, 1H), 8.07 (d, ^3J = 7.6 Hz, 1H), 7.82 (d, ^3J =7.2 Hz, 1H), 7.61 (dd, ^3J = 8.4 Hz, ^3J = 7.6 Hz, 1H). 7.46 (d, ^3J= 7.2 Hz, 1H), 3.12 (t, ^3J =8.0 Hz, 2H), 2.72 (s, acetyl-CH_3, 3H). 1.76-1.68 (m, 2H), 1.51-1.41 (m, 2H), 0.98 (t, ^3J = 7.2 Hz, 3H). ^{13}C NMR (150 MHz, $CDCl_3$) 200.9, 148.7, 143.5, 135.2, 133.8, 129.8, 128.4, 126.3, 125.1, 124.5, 121.9, 33.5, 33.0, 28.5, 22.8, 14.0. HRMS (ESI) m/z: $[M + H]^+$ Calculated for $C_{16}H_{18}NO_3$: 272.1287. Found : 272.1290.

Synthesis of BuPNI

Into a 50 mL round-bottomed flask, 100 mg (0.37 mmol) of compound **2** was loaded along with 10 mL of ethanol and the reaction vessel was placed inside an oil bath. While gradually heating up the solution to 80 °C, B_2pin_2 (201 mg, 0.79 mmol) and KF (106 mg 1.84 mmol) were added in succession. The mixture was refluxed for 16 h. After cooling down to room temperature, ethanol was removed under reduced pressure. The dry residue was subsequently washed with water (3 x 20 mL), EtOH (3 x 10 mL) and Et_2O (3 x5 mL). The crude mixture was then purified via column chromatography using DCM/hexane as eluent (v/v = 1 : 2 to 1 : 1). The desired compound BuPNI was obtained as as blue-brown solid. Yield = 41.0 mg (47%). ^{1}H NMR (400MHz, $CDCl_3$) δ = 12, 48 (br,1H, -OH), 8.54 (d, ^3J = 7.60 Hz, 1H), 7.97 (d, ^3J = 8.40 Hz, 1H), 7.94 (d, ^3J = 7.20 Hz, 1H), 7.81 (d, ^3J = 7.60 Hz, 1H), 7.66 (d, ^3J = 8.00 Hz, 1H), 7.63 (d, ^3J = 7.60 Hz, 1H), 7.58 (d, ^3J = 8.40 Hz, 1H), 7.51-7.46 (m, 2H), 7.16 (s, 1H), 7.16 (d, ^3J = 7.20 Hz, 1H), 3.19 (t, ^3J = 7.60 Hz, 2H), 3.10 (t, ^3J = 7.60 Hz, 2H), 1.83-1.73 (m, 4H), 1.52-1.42 (m, 4H), 1.00 (t, ^3J = 7.20 Hz, 3H), 0.9 (t, ^3J = 7.20 Hz, 3H) ppm. ^{13}C NMR (150 MHz, $CDCl_3$) 179.6, 155.5, 153.8, 149.6, 144.9, 143.1, 139.0, 132.6, 131.6, 129.7, 129.6, 128.9, 128.6, 128.0, 127.6, 127.6, 127.3, 126.0, 124.5, 122.6, 121.5, 117.3, 108.4, 90.5, 34.1, 33.9, 33.8, 32.4, 23.0, 22.9, 14.1, 14.1 ppm. HRMS (ESI) m/z: $[M + H]^+$ Calculated for $C_{32}H_{31}N_2O_2^+$: 475.2386; Found: 475.2379; IR 2953, 2929, 2858, 1651, 1598, 1570, 1520, 1476, 1448, 1399, 1374, 1357, 1282, 1207, 1179, 1043, 911, 856, 805, 776, 741, 691, 632 cm^{-1}. UV-vis ($CHCl_3$) λ_{max}/nm (ε/$M^{-1}cm^{-1}$) 638 (30400). mp 190°C.

3. ^{1}H and ^{13}C Spectra

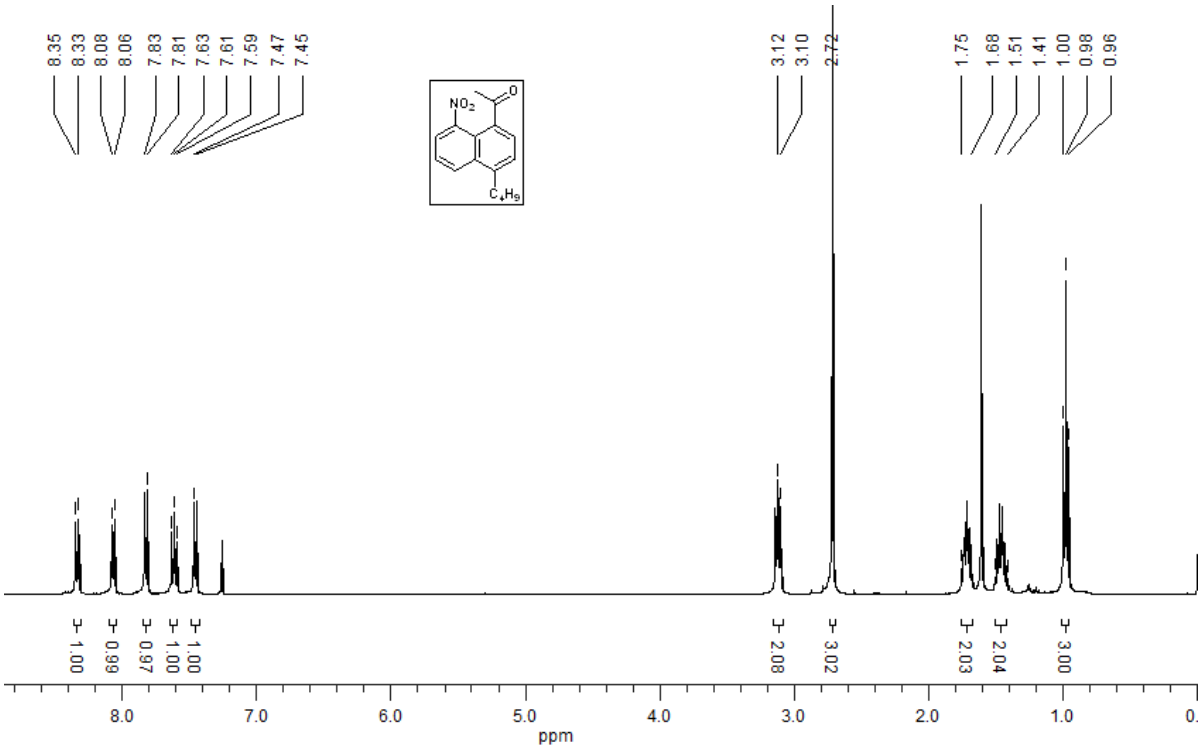

Figure S1. ^{1}H NMR (400 MHz, 298 K) spectrum of **2** in $CDCl_3$.

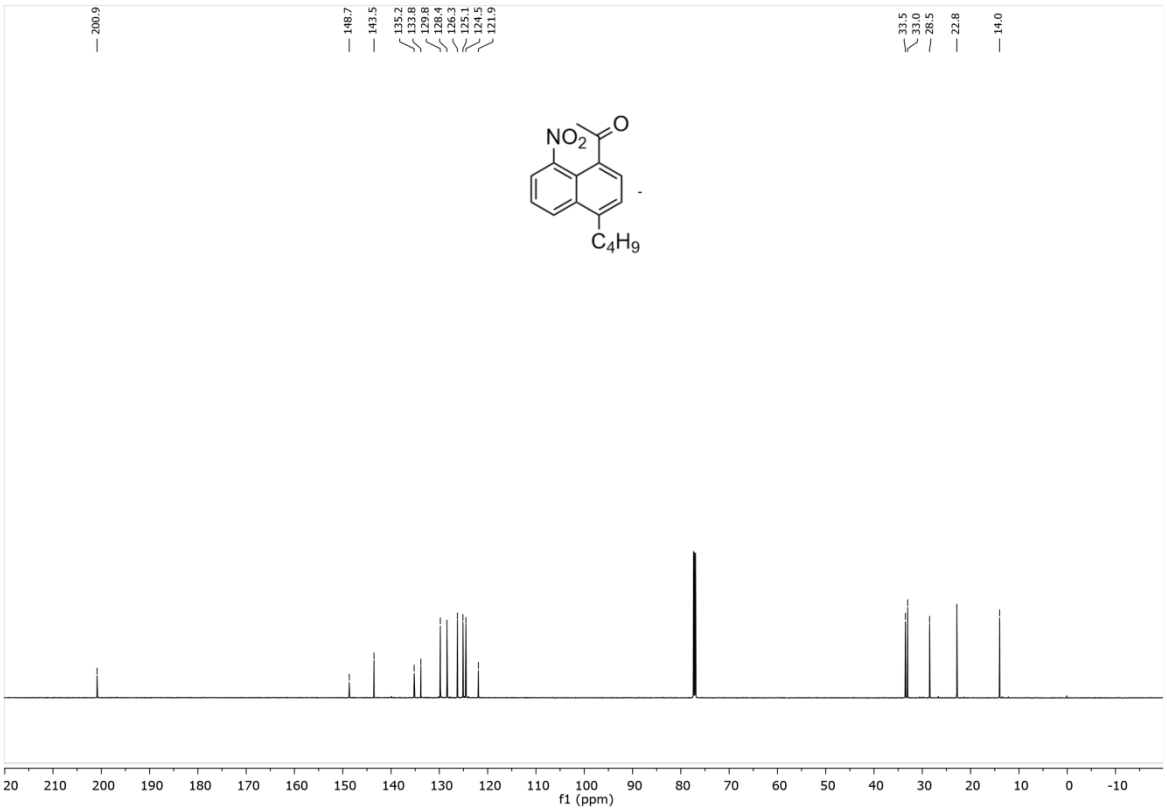

Figure S2. ^{13}C NMR (150 MHz, 298 K) spectrum of compound **2** in $CDCl_3$.

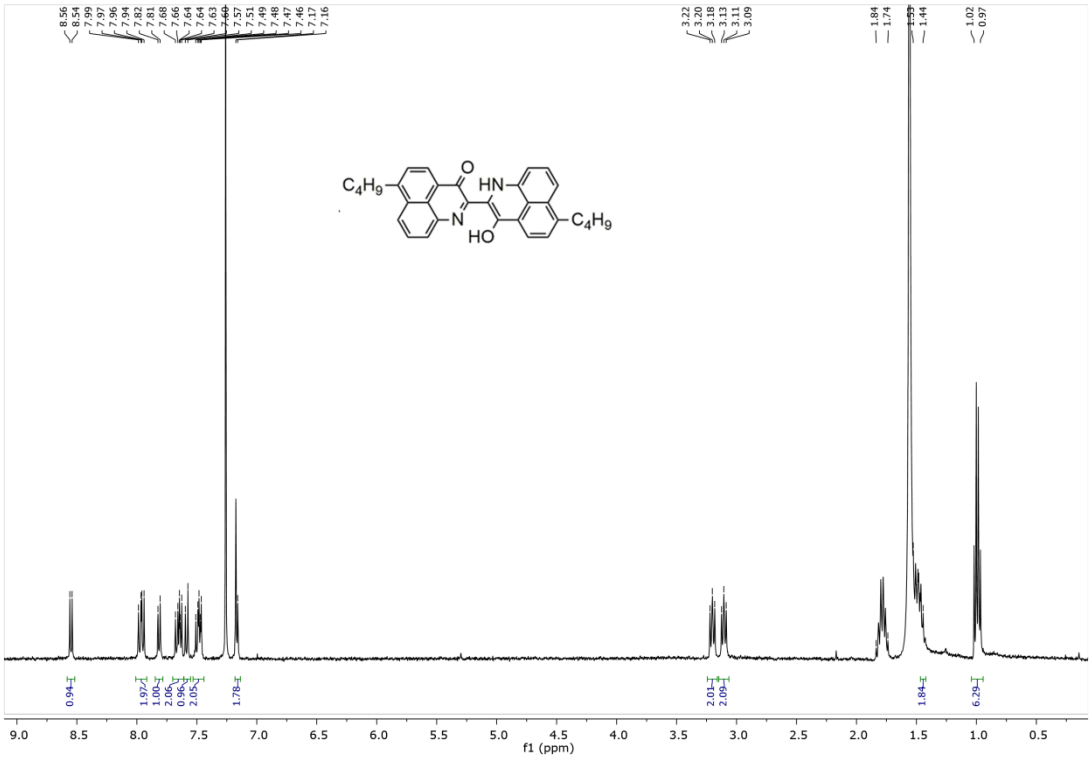

Figure S3. ^{1}H NMR (400 MHz, 298 K) spectrum of BuPNI in $CDCl_3$.

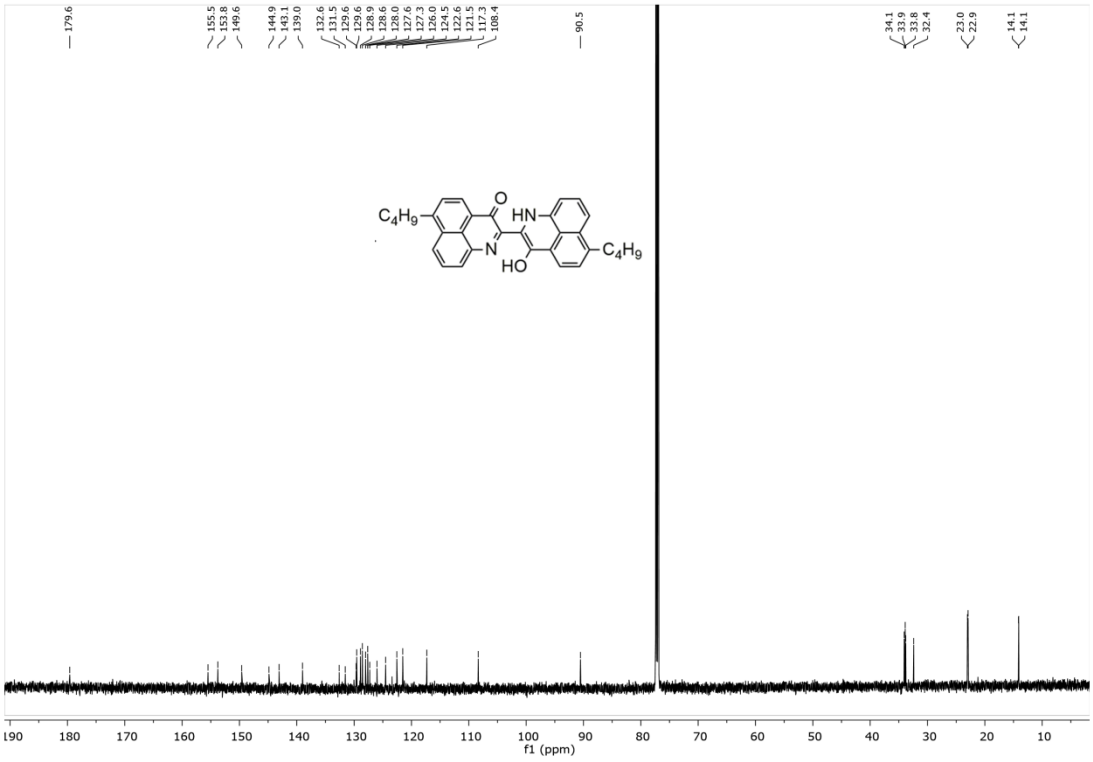

Figure S4. ^{13}C NMR (150 MHz, 298 K) spectrum of BuPNI in $CDCl_3$.

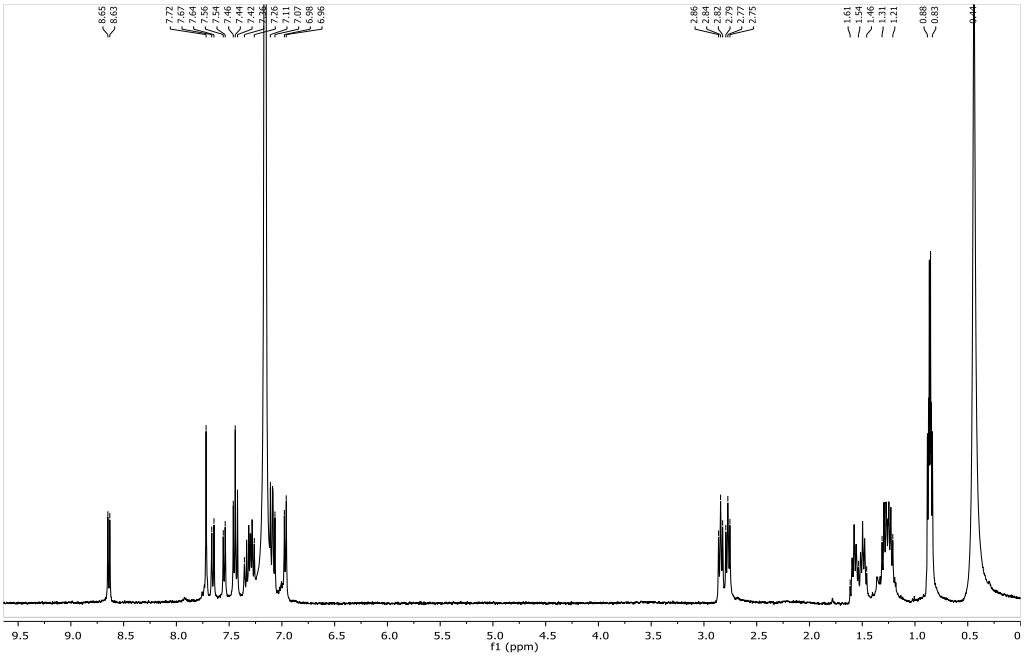

Figure S5. ^{1}H NMR (400 MHz, 298 K) spectrum of BuPNI in C_6D_6.

4. High resolution mass spectrometry (HRMS)

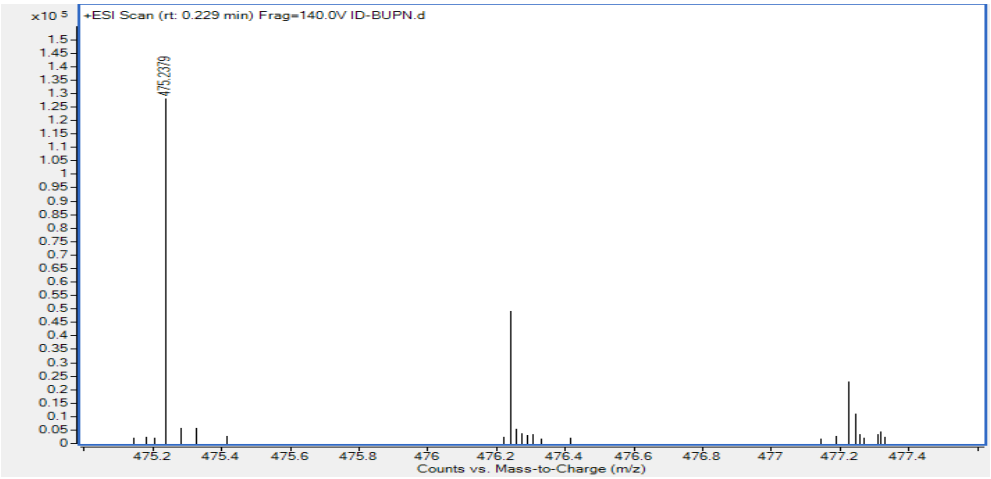

Figure S6. HRMS (ESI) spectrum of $[BuPNI + H]^+$.

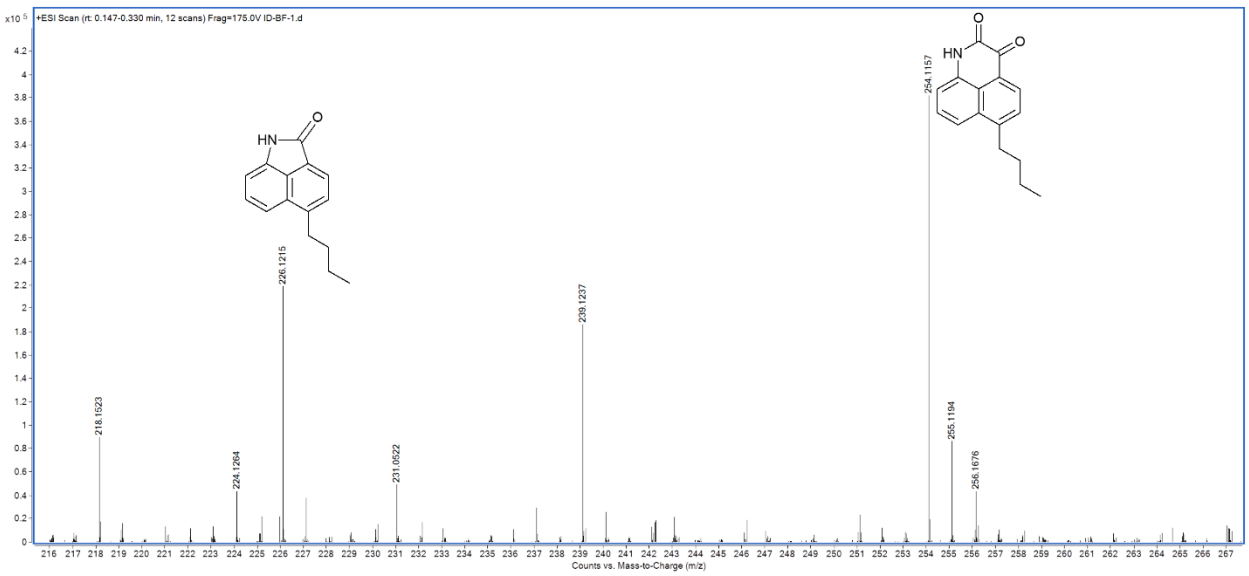

Figure S7. HRMS (ESI) spectrum of a reaction mixture after mixing BuPNI (60 μM) and C60 (300 μM) in toluene at room temperature for 6 d.

Indigo is known to undergo oxidative decomposition to produce isatin, which subsequently converted in to anthranilic acid (Scheme S2b).[2] A similar decomposition pathway was followed for BuPNI in the presence of C60. Fullerene (C60) is well known to produce active oxygen species, which enhance photo-decomposition of organic dye.[3] The decomposition pathway of BuPNI is summarized in Scheme S2.

Scheme S2. Oxidative decomposition of BuPNI in presence of C60 in toluene

(a) Decomposition of BuPNI

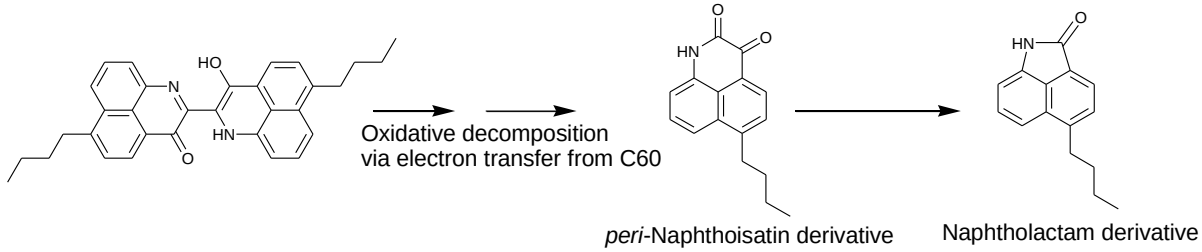

(b) Decomposition of indigo[2]

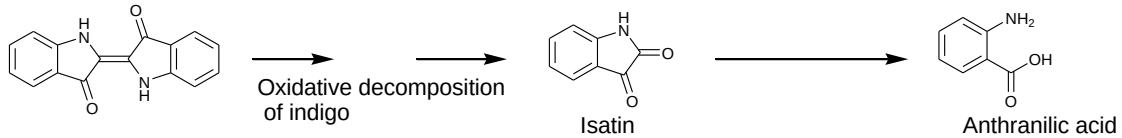

5. Absorption and photoluminescence spectroscopy

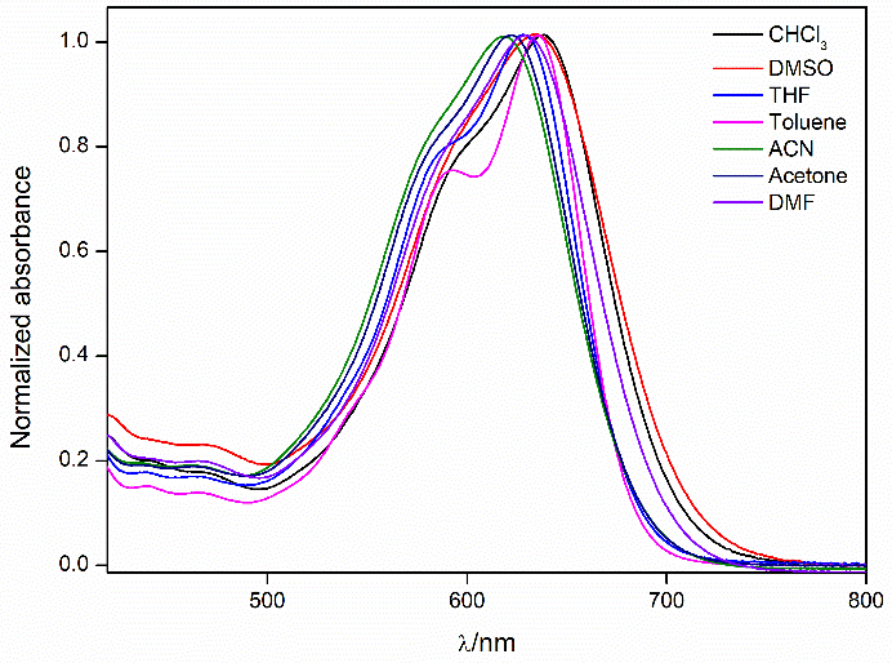

Figure S8. Normalized absorption spectra (298 K) of BuPNI in different solvents (c ~ 5). Samples were prepared by dissolving the required amount of compounds in volumetric flask. The solution was used instantly for spectroscopic measurements.

Table S1. Absorption and photoluminescence properties of BuPNI in different solvents.

Solvents	**λ_{abs}(nm)**	**λ_{ems} (nm)**
Acetonitrile	619	748
Acetone	622	736
THF	628	706
DMF	629	752
DMSO	635	762
Toluene	636	691
$CHCl_3$	638	745
MCH	633	648

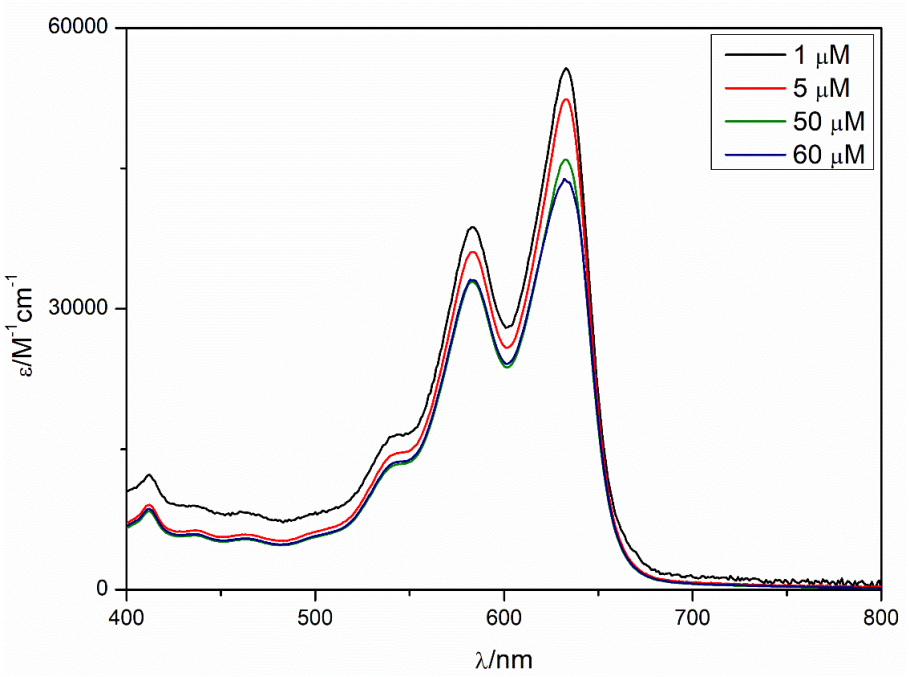

Figure S9. Concentration dependent (c ~ 1– 60 μM) absorption spectra (298 K) of BuPNI in MCH. To avoid precipitation of the aggregates, freshly prepared solutions were used for investigations.

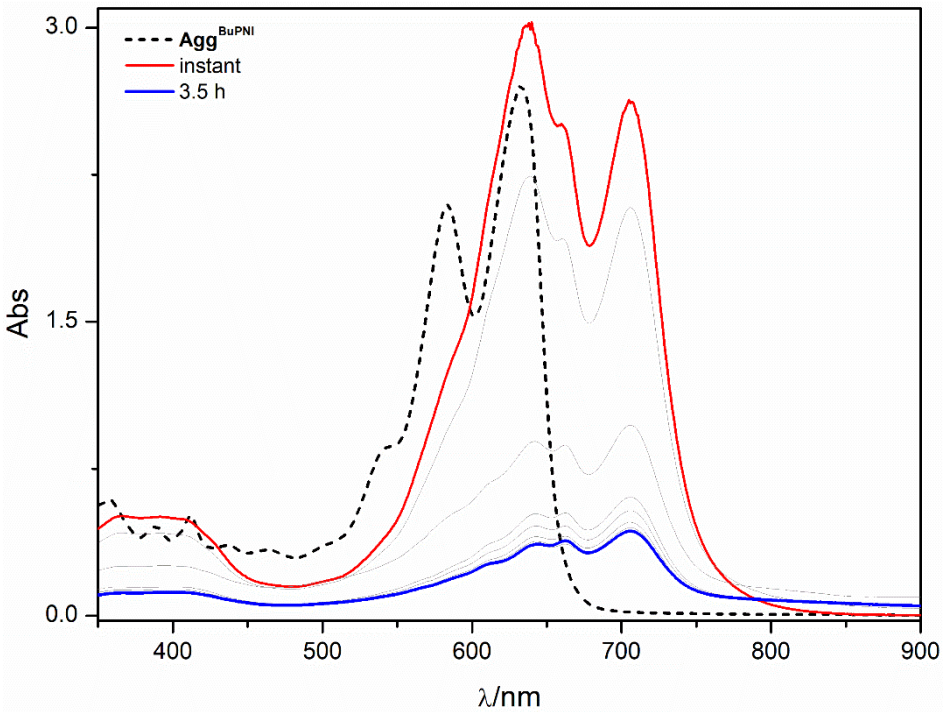

Figure S10. Absorption spectra of instantly prepared TFA⊂**Agg**$^{\mathbf{BuPNI}}$ (red line) in MCH (c ~ 60 μM) and its evolution with time. Substantial change in A_{706}/A_{644} value was observed after 3.5 h (blue line). UV-vis spectrum of **Agg**$^{\mathbf{BuPNI}}$ (black dash) in MCH (c ~ 60 μM) is included for comparison.

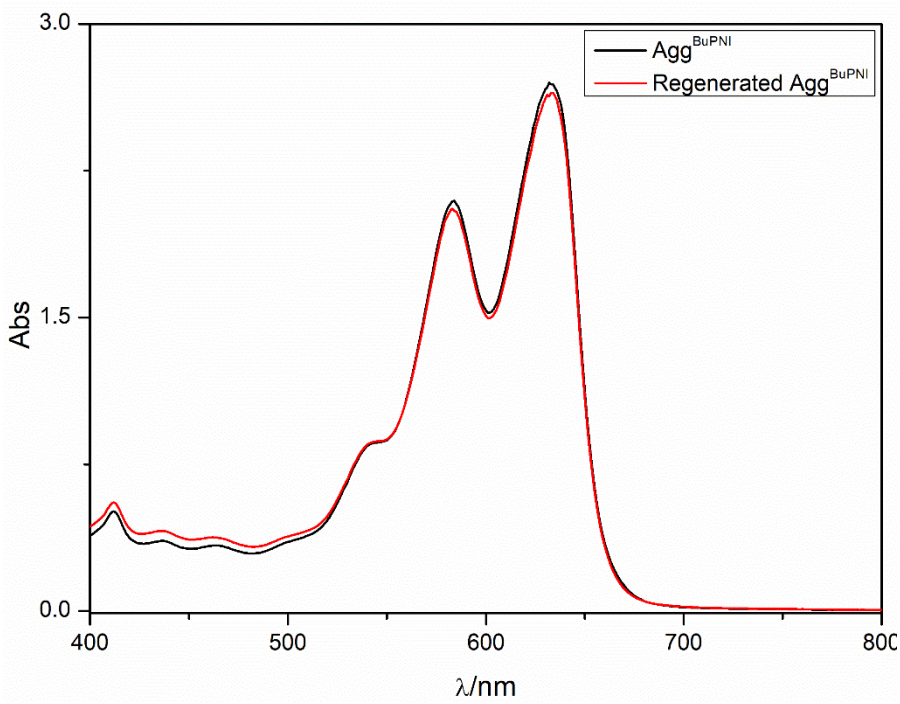

Figure S11. Absorption spectra of freshly prepared **Agg**$^{\mathbf{BuPNI}}$ (black) and regenerated **Agg**$^{\mathbf{BuPNI}}$ (red) after treatment of TFA⊂**Agg**$^{\mathbf{BuPNI}}$ with Et_3N in MCH (c ~ 60 μM) at 298 K.

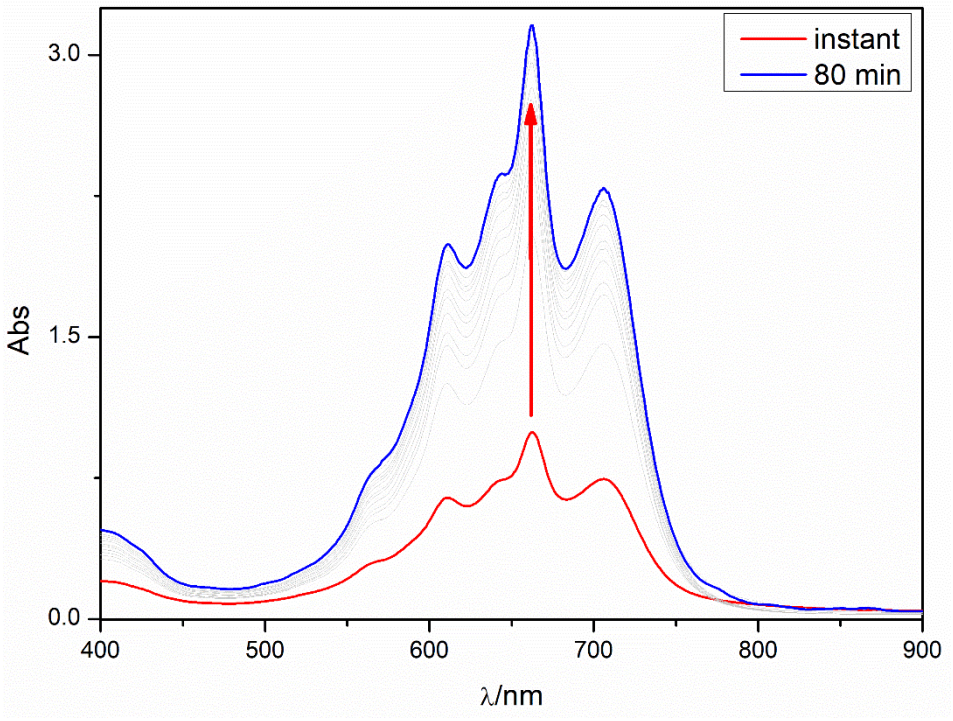

Figure S12. Time dependent absorption spectra of TFA⊂**Agg**$^{\mathbf{BuPNI}}$ in MCH (c ~ 60 μM) at 333 K. The sample was prepared by treating a freshly prepared solution of **Agg**$^{\mathbf{BuPNI}}$ with TFA. After completion of the supramolecular rearrangement process (3.5 h), the sample was heated to 333 K and the changes were recorded at different times keeping the temperature fixed. Due to dissolution of the large aggregates, the absorption value increased.

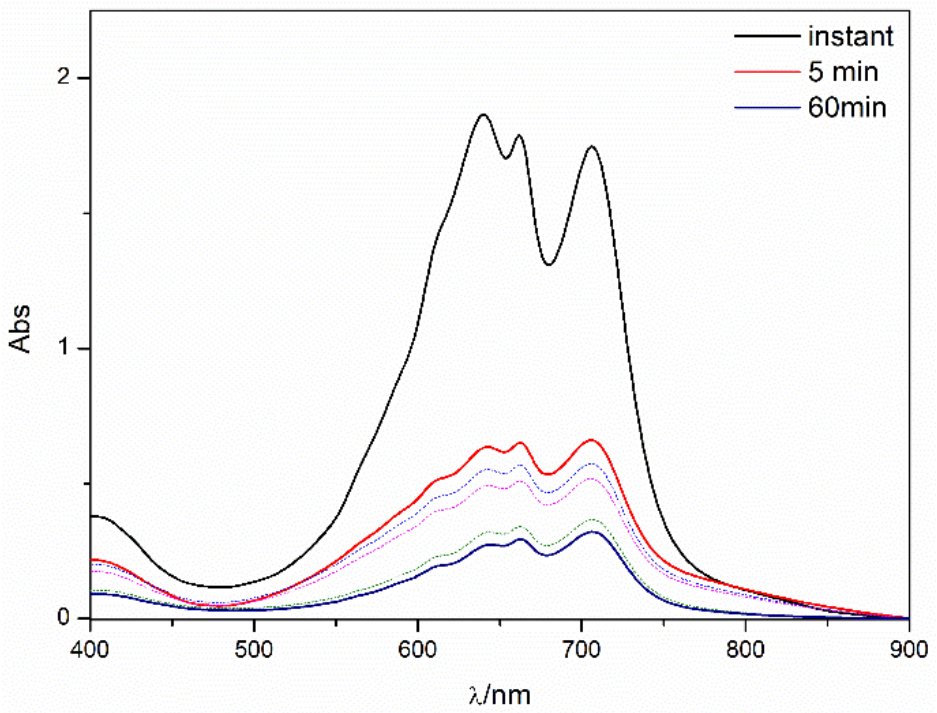

Figure S13. Time dependent Absorption spectra of TFA⊂**Agg**$^{\mathbf{BuPNI}}$ (c ~ 60 μM) at 298 K in MCH. A solution of TFA-trapped aggregate TFA⊂**Agg**$^{\mathbf{BuPNI}}$ (3.5 h old sample) was heated to 333 K, and subsequently cooled down to 298 K. The changes were recorded at different times keeping the solution at room temperature.

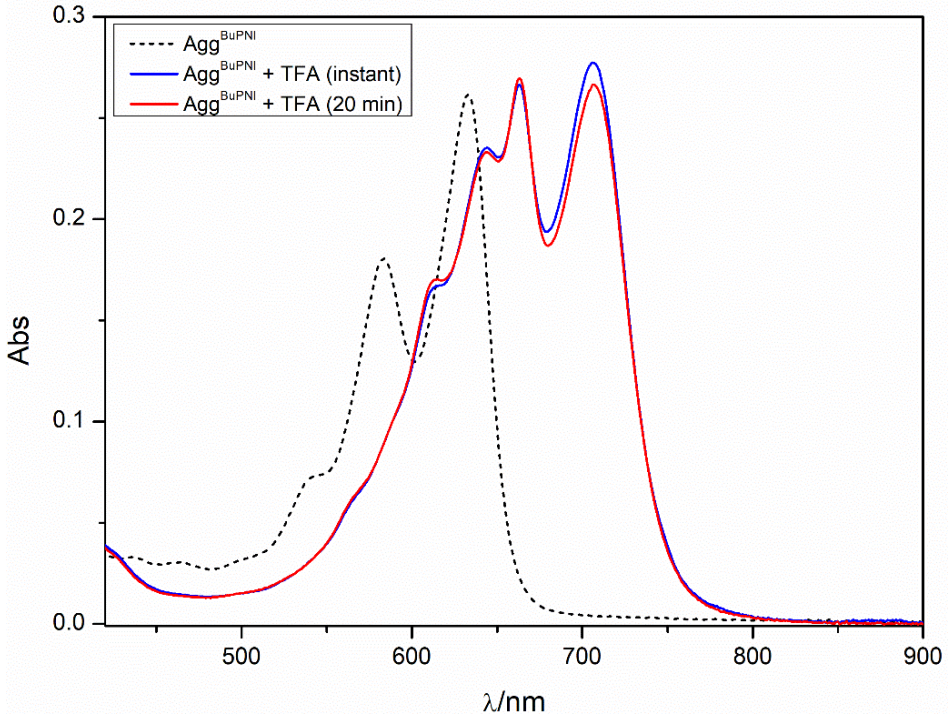

Figure S14. Absorption spectra of instantly prepared TFA⊂Agg$^{\mathrm{BuPNI}}$ (blue line) in MCH (c ~ 5 μM) and its evolution with time. No significant changes were noticed after 20 min (red line). UV-vis spectrum of Agg$^{\mathrm{BuPNI}}$ (black dash) in MCH (c ~ 5 μM) is included for comparison.

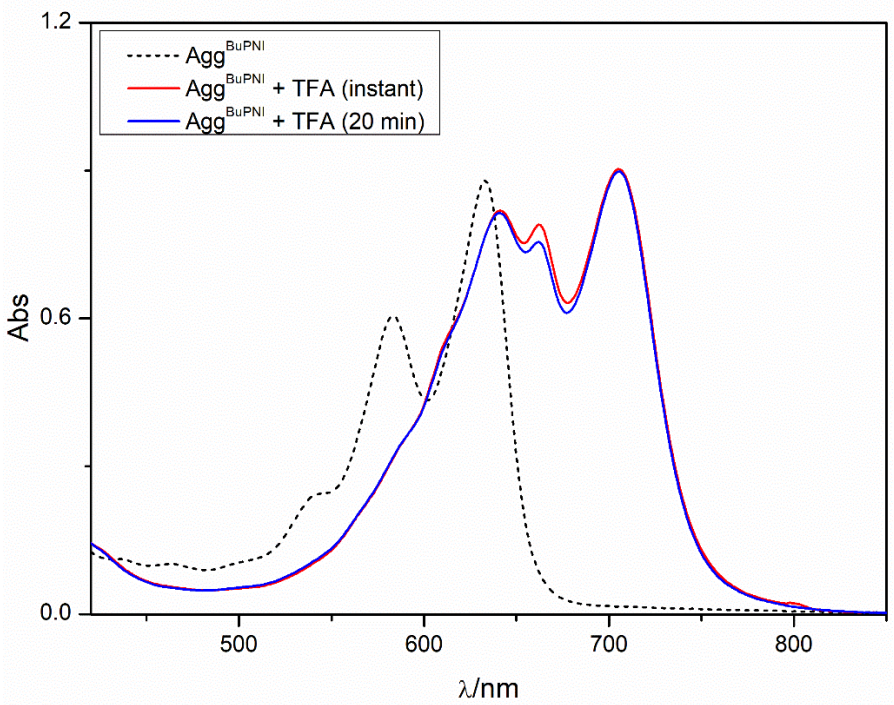

Figure S15. Absorption spectra of instantly prepared TFA⊂Agg^{BuPNI} (red line) in MCH (c ~ 20 μM) and its evolution with time. No significant changes were noticed after 20 min (blue line). UV-vis spectrum of Agg^{BuPNI} (black dash) in MCH (c ~ 20 μM) is included for comparison.

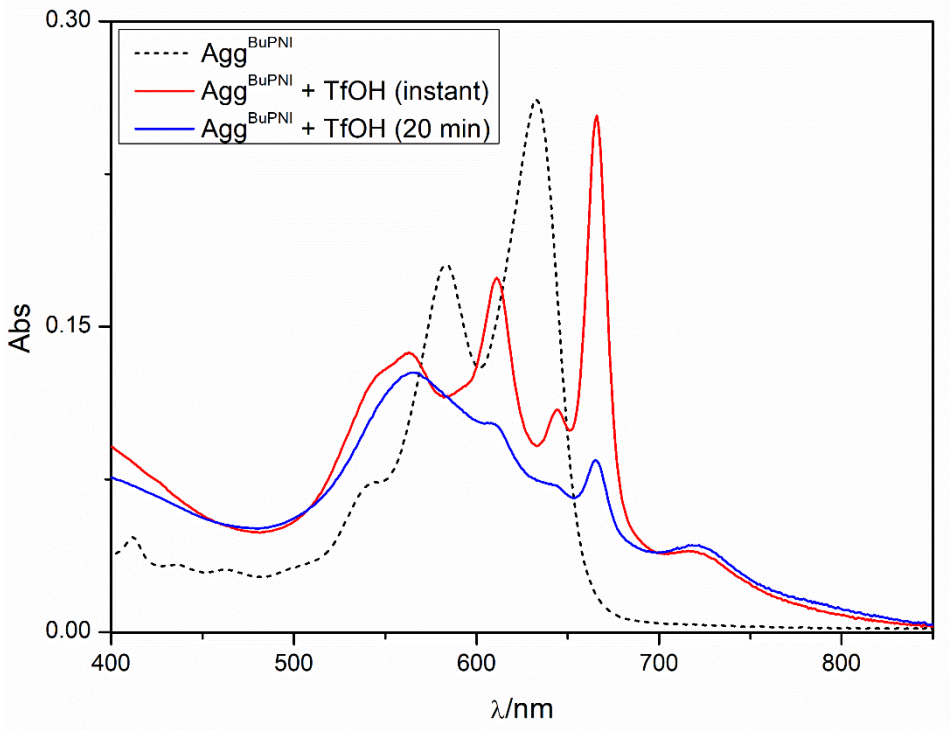

Figure S16. Absorption spectra of instantly prepared TfOH⊂**Agg^{BuPNI}** (red line) in MCH (c ~ 5 μM) and its evolution with time. Significant drop in the absorbance was observed after 20 min (blue line) due to supramolecular rearrangement. UV-vis spectrum of Agg^{BuPNI} (black dash) in MCH (c ~ 5 μM) is included for comparison.

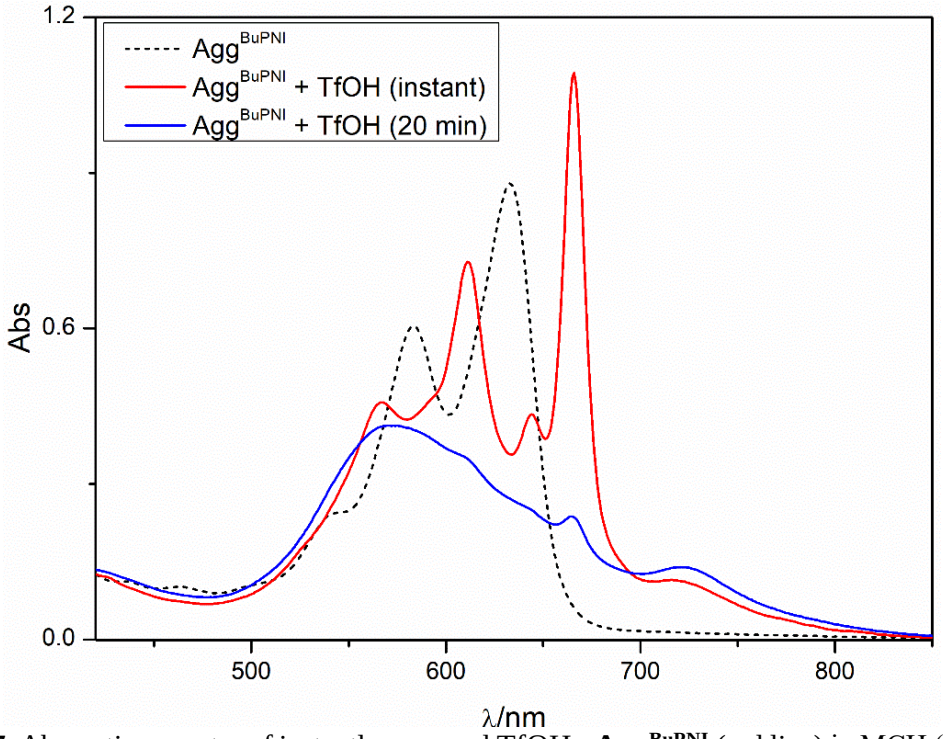

Figure S17. Absorption spectra of instantly prepared TfOH⊂**Agg^{BuPNI}** (red line) in MCH (c ~ 20 μM) and its evolution with time. Significant drop in the absorbance was observed after 20 min (blue line) due to supramolecular rearrangement. UV-vis spectrum of Agg^{BuPNI} (black dash) in MCH (c ~ 20 μM) is included for comparison.

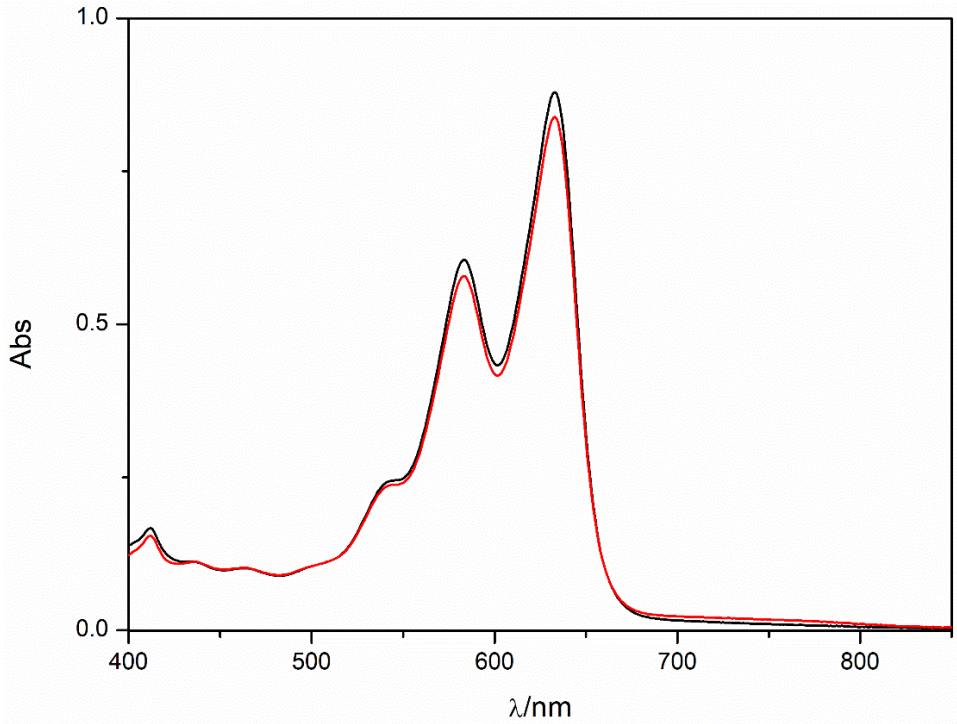

Figure S18. Absorption spectra of freshly prepared **Agg^{BuPNI}** (black) and regenerated **Agg^{BuPNI}** (red) after treatment of TfOH⊂**Agg^{BuPNI}** with Et_3N in MCH (c ~ 20 μM) at 298 K.

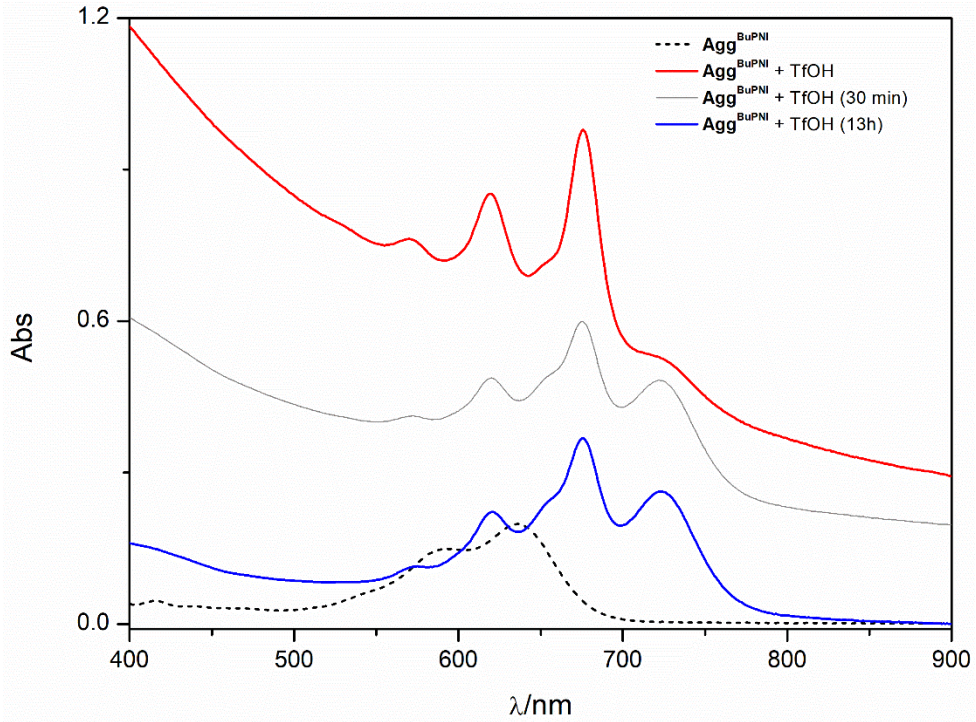

Figure S19. Supramolecular rearrangement of **Agg^{BuPNI}** in presence of TfOH in toluene at a concentration of 5 μM. The original spectrum of **Agg^{BuPNI}** (dash) showed substantial changes with time (solid lines).

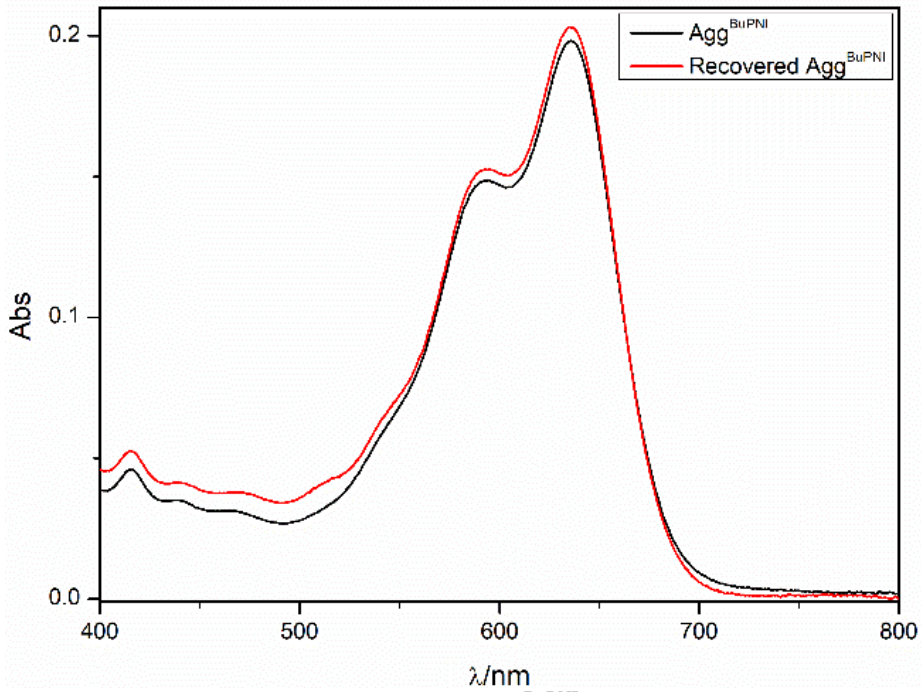

Figure S20. Absorption spectra of freshly prepared **Agg^{BuPNI}** (black) and regenerated **Agg^{BuPNI}** (red) after treatment of TfOH⊂**Agg^{BuPNI}** with Et_3N in toluene (c ~ 5 μM) at 298 K.

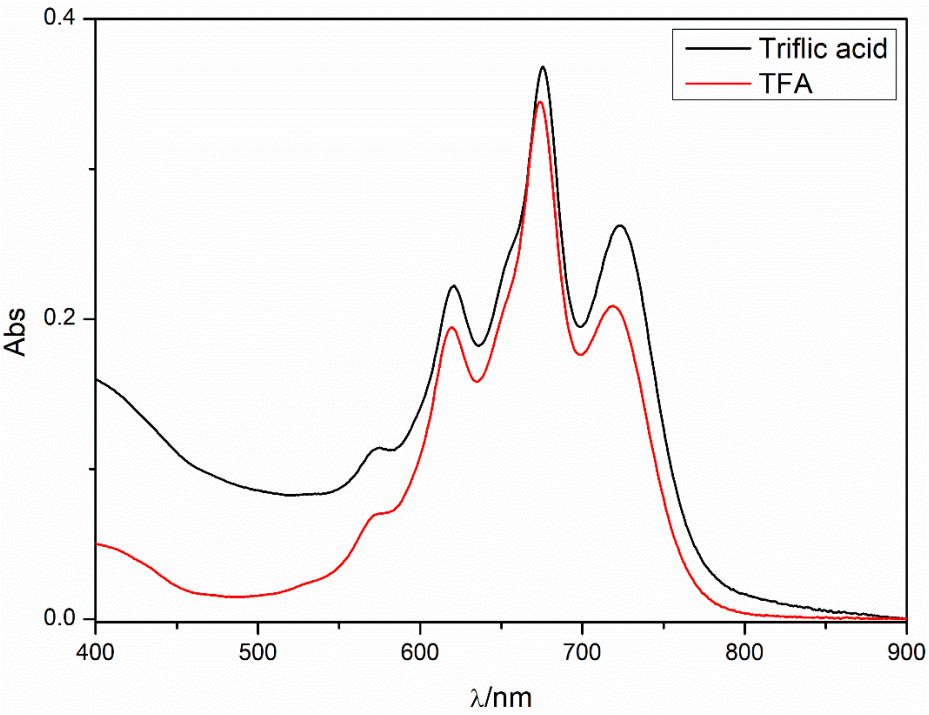

Figure S21. A comparison of the absorption spectrum of TFA⊂**Agg**$^{\mathbf{BuPNI}}$(red) and TfOH⊂**Agg**$^{\mathbf{BuPNI}}$ (black) in toluene (c ~ 5 μM) at 298 K. Similar spectral features suggested that in toluene both the guests induced comparable rearrangement.

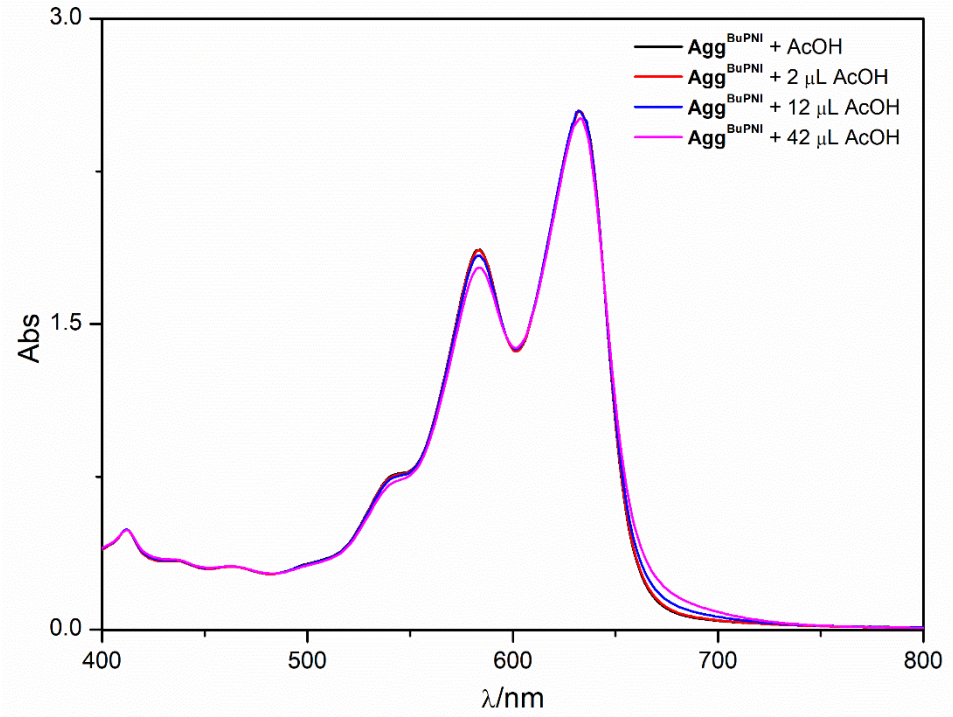

Figure S22. Absorption spectra of **Agg**$^{\mathbf{BuPNI}}$ (50 μM) in MCH after addition of AcOH. Less solvophobic guest AcOH did not bring changes in the supramolecular rearrangement process.

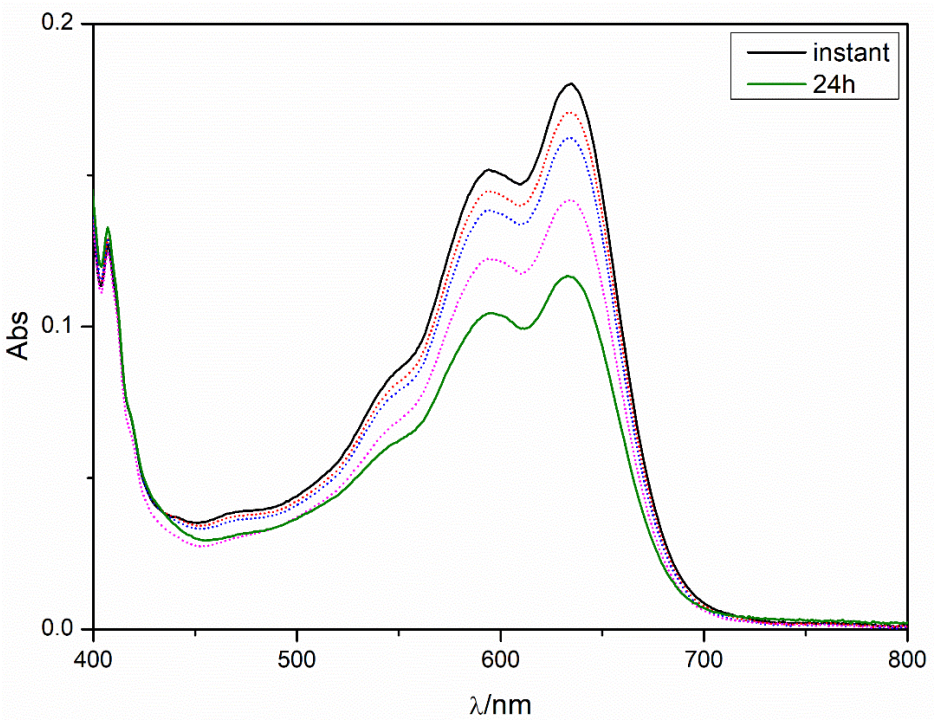

Figure S23. Time dependent absorption spectra of C60-**Agg**$^{\mathbf{BuPNI}}$ in toluene (c ~ 5 µM). Steady decrease in absorbance indicates decomposition of BuPNI, evidenced from mass spectrometry (Figure S7).

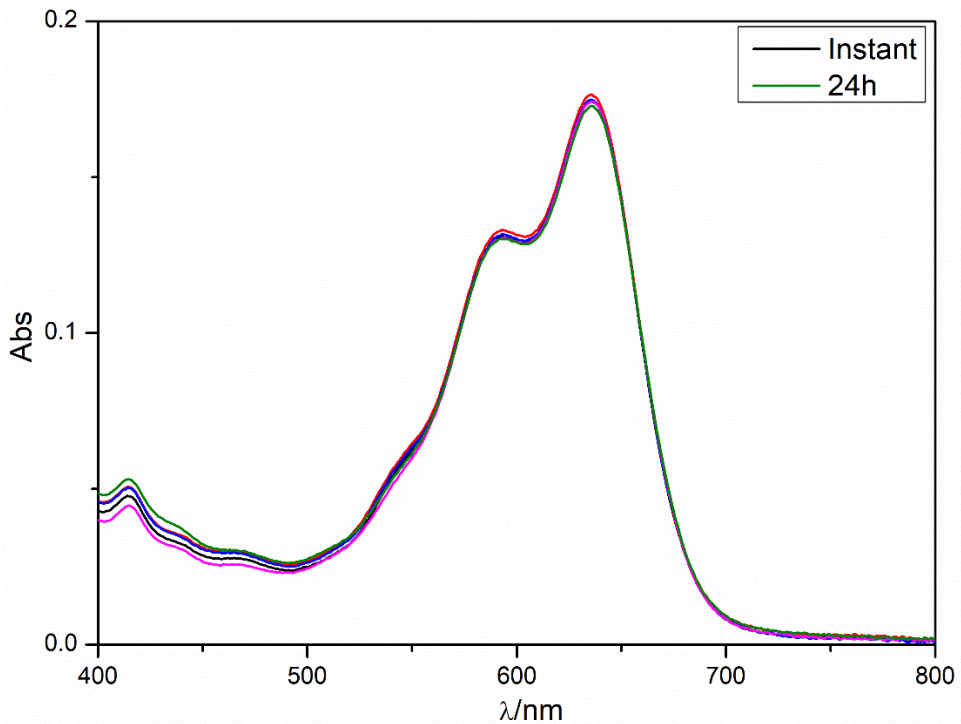

Figure S24. Time dependent absorption spectra **Agg**$^{\mathbf{BuPNI}}$ in toluene (c ~ 5 µM). The spectra remain unchanged over 24 h, suggesting the dye assembly is stable in toluene.

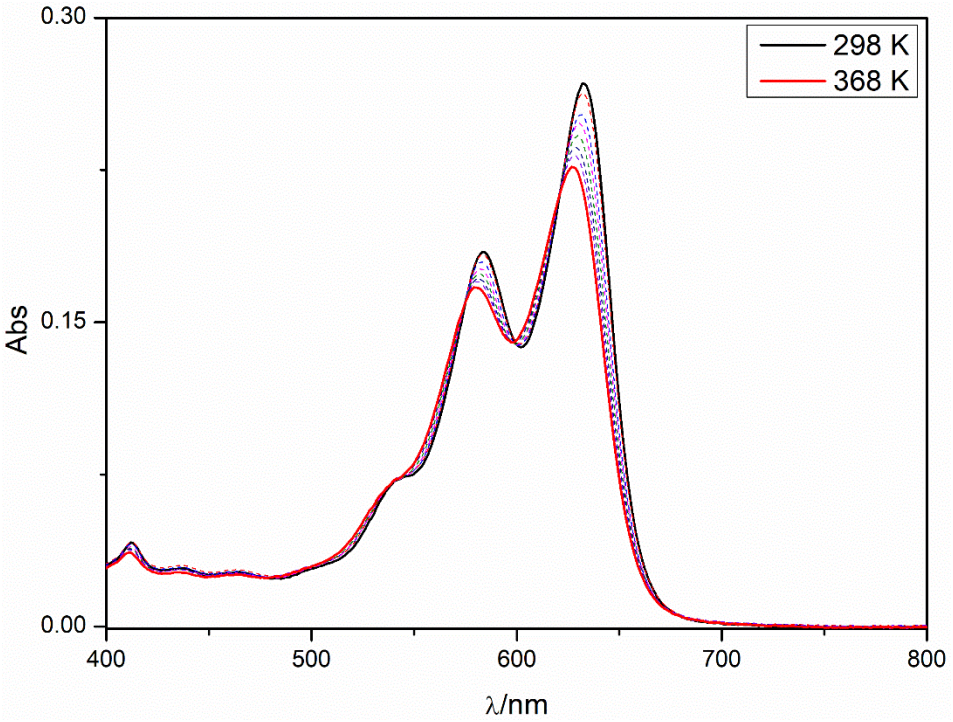

Figure S25. Variable temperature absorption spectra of **Agg**$^{\mathbf{BuPNI}}$ (5 µM) in a MCH/toluene soluiton (v/v = 95/5). Spectral changes were similar with that of the changes observed in pure MCH (Fig. 2c), confirmed similar aggregation behavior in both the cases.

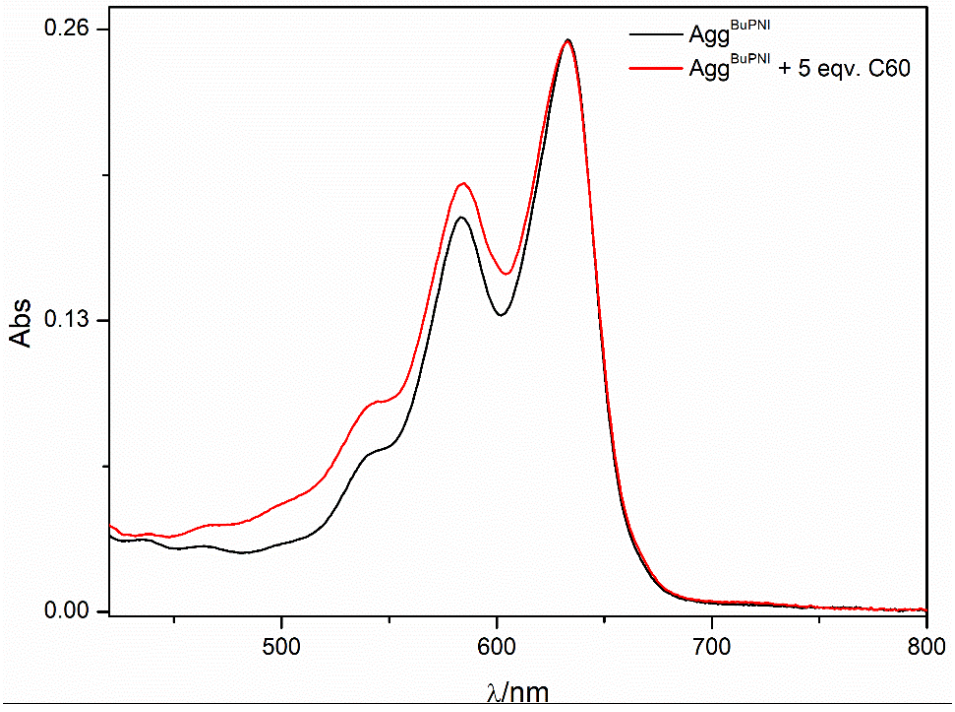

Figure S26. Spectral changes during supramolecular rearrangement of **Agg**$^{\mathbf{BuPNI}}$ in the presence of C60 fullerene. Almost similar spectrum, **Agg**$^{\mathbf{BuPNI}}$ (black) and C60-**Agg**$^{\mathbf{BuPNI}}$ (red) in MCH/toluene (v/v = 95/5), suggested negligible interaction in the ground state. Experiment was carried out by adding 5 equivalent of C60 fullerene solution (in toluene) to the solution of **Agg**$^{\mathbf{BuPNI}}$ (5 µM) in a MCH/toluene mixture (v/v = 95/5).

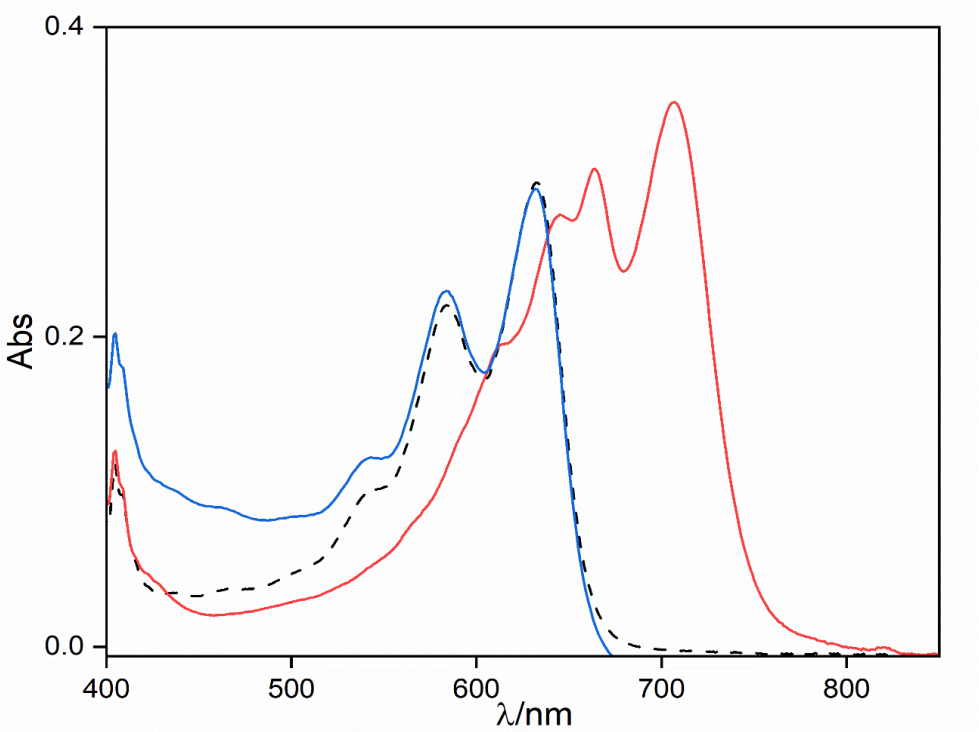

Figure S27. Spectral change during switching between C60-**Agg**$^{\mathbf{BuPNI}}$ and TFA⊂ **Agg**$^{\mathbf{BuPNI}}$ in a 95/5 (v/v) mixture of MCH-toluene (c ~ 5 µM). Freshly prepared C60-**Agg**$^{\mathbf{BuPNI}}$ (black dash) was converted in to TFA⊂ **Agg**$^{\mathbf{BuPNI}}$ (red line) after addition of TFA. The aggregate C60-**Agg**$^{\mathbf{BuPNI}}$ was regenerated after addition of Et_3N (blue line).

Remote acidification and subsequent removal of acid

Diffusion through a bilayer between two immiscible solvents was chosen as the process for both acidification and the removal of acid. The organic layer was initially placed on top of the acid-water solution, and after the maximum permissible acid moves through, the acid layer was replaced with deionized water. The strength of acid used was 10 % TFA in water (v/v).

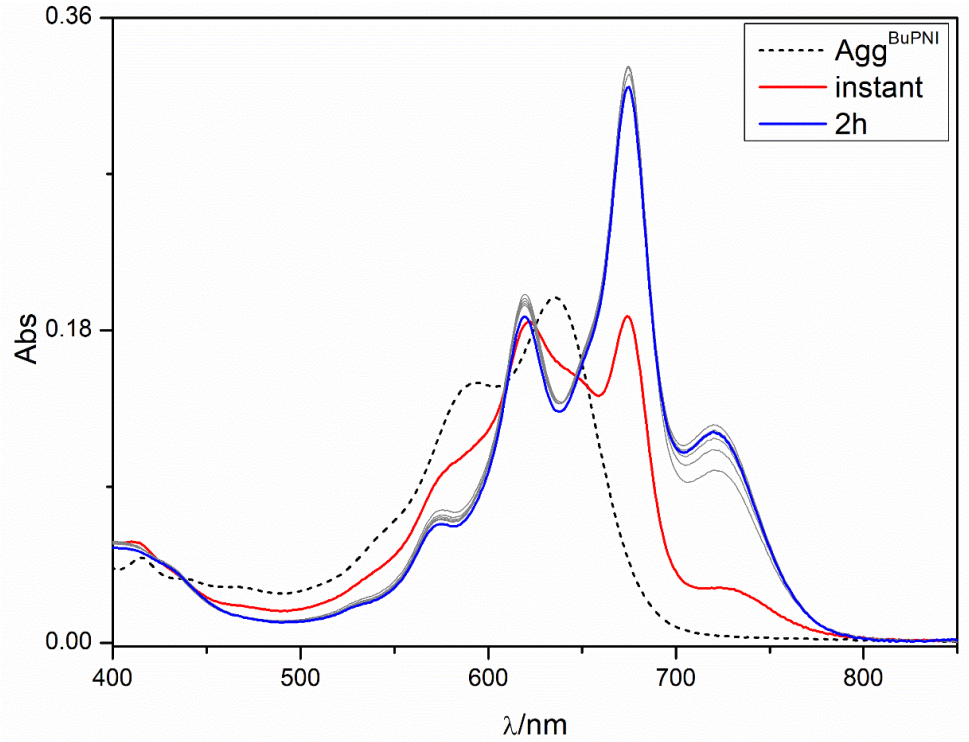

Figure S28. Spectral change during rearrangement of **Agg**$^{\mathbf{BuPNI}}$ (black dash) to TFA⊂**Agg**$^{\mathbf{BuPNI}}$ (solid line) via diffusion of TFA from the aqueous layer to the organic layer (toluene) at a dye concentration 5 µM. No noticeable changes could be seen after 2 h.

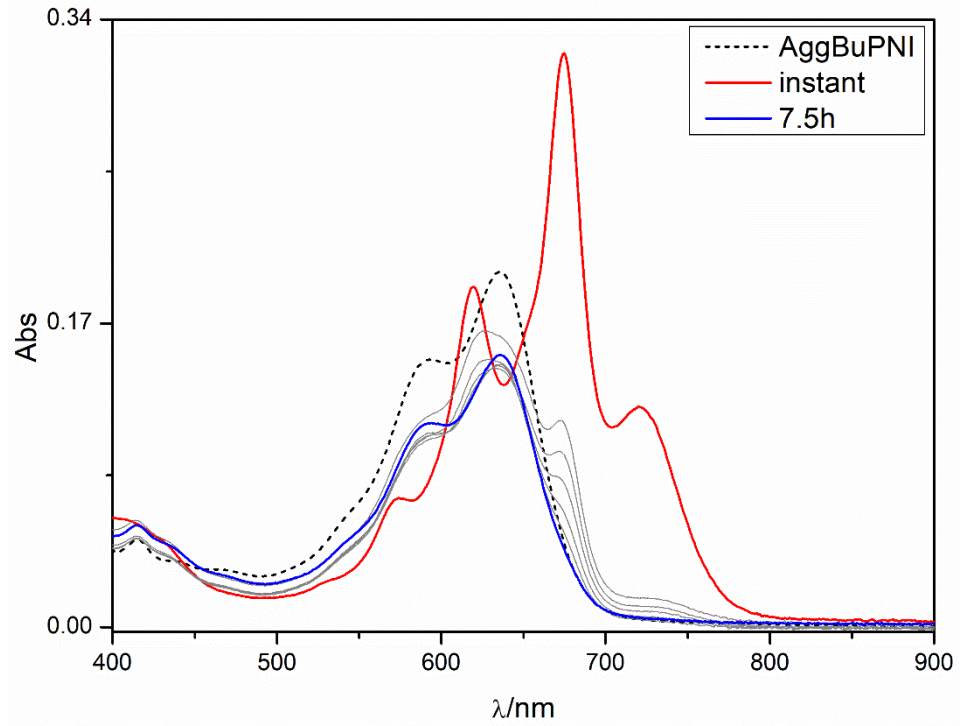

Figure S29. Spectral change during rearrangement of TFA⊂**Agg**$^{\mathbf{BuPNI}}$ to **Agg**$^{\mathbf{BuPNI}}$ via diffusion of TFA from the organic layer (toluene) to the aqueous layer at a dye concentration 5 µM. The spectrum of TFA⊂**Agg**$^{\mathbf{BuPNI}}$ (red line, marked as instant), generated in the previous experiment (Figure S28) was used as starting point in the current experiment. Time dependent diffusion showed the regeneration of original aggregate **Agg**$^{\mathbf{BuPNI}}$.

Scheme S3. Schematic diagram for supramolecular switching between TFA⊂**Agg**$^{\mathbf{BuPNI}}$ and C60-**Agg**$^{\mathbf{BuPNI}}$ via change in acidic strength at a remote aqueous layer.

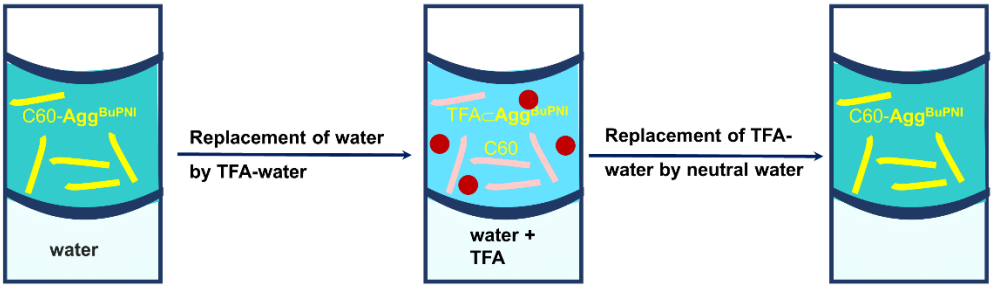

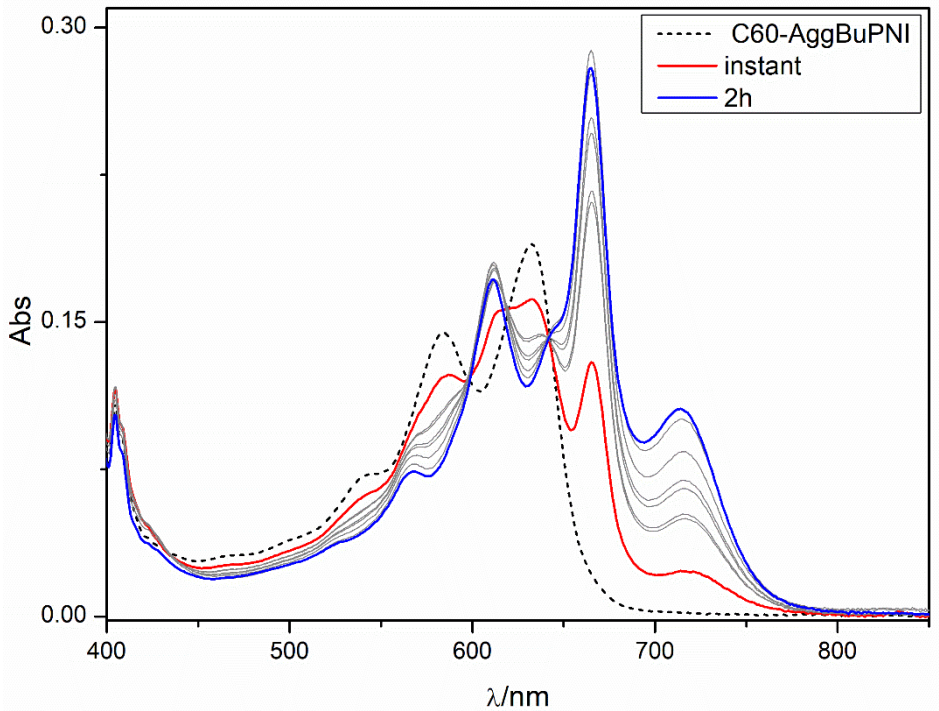

Figure S30. Spectral changes during dis-assembly of C60-**Agg**$^{\mathbf{BuPNI}}$ and formation of TFA⊂**Agg**$^{\mathbf{BuPNI}}$ via TFA diffusion from the aqueous layer to the organic layer (95/5 v/v mixture of MCH-toluene) at a dye concentration 5 μM. The experiment was carried out by preparing a solution of C60-**Agg**$^{\mathbf{BuPNI}}$ in 95/5 v/v mixture of MCH-toluene. Immediately after placing the solution over aq. TFA solution showed the formation of TFA⊂**Agg**$^{\mathbf{BuPNI}}$ (red line, instant). Course of the supramolecular changes was monitored and the spectrum were recorded (solid line). No further changes could be seen after 2 h.

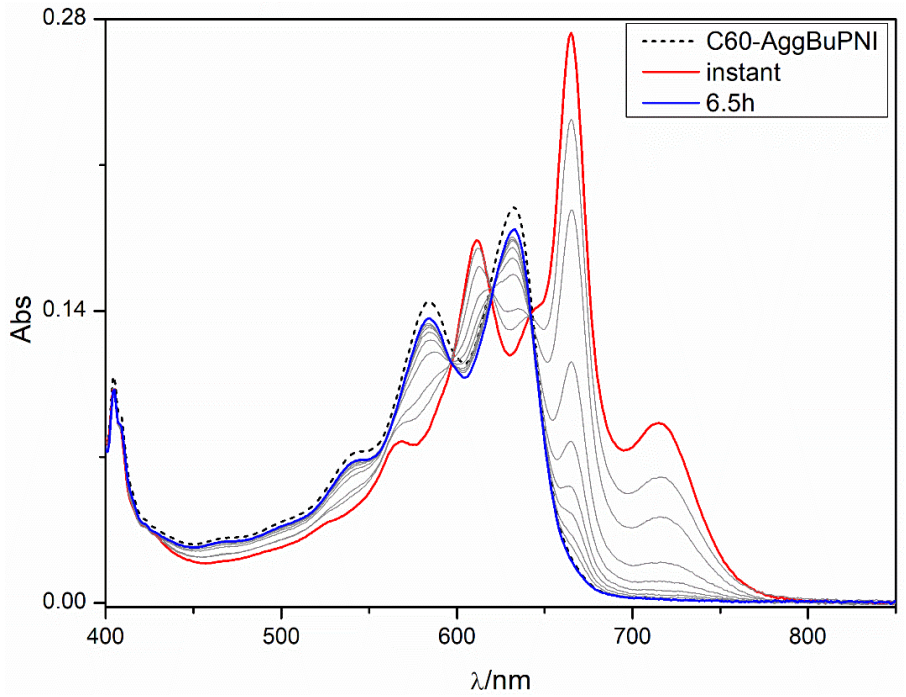

Figure S31. Spectral changes during dis-assembly of TFA⊂**Agg**$^{\mathbf{BuPNI}}$ and formation of C60-**Agg**$^{\mathbf{BuPNI}}$ via TFA diffusion from the organic (95/5 v/v mixture of MCH-toluene) layer to the aqueous layer at a dye concentration 5 μM. The aggregate TFA⊂**Agg**$^{\mathbf{BuPNI}}$ was prepared by diffusing TFA from the aqueous layer to the organic layer over a period of 2 h (previous experiment, **Figure S30**). The acidic-aqueous layer was then replaced with neutral water and the changes were recorded spectroscopically (solid line). Generation of C60-**Agg**$^{\mathbf{BuPNI}}$ completed after 6.5 h (blue line).

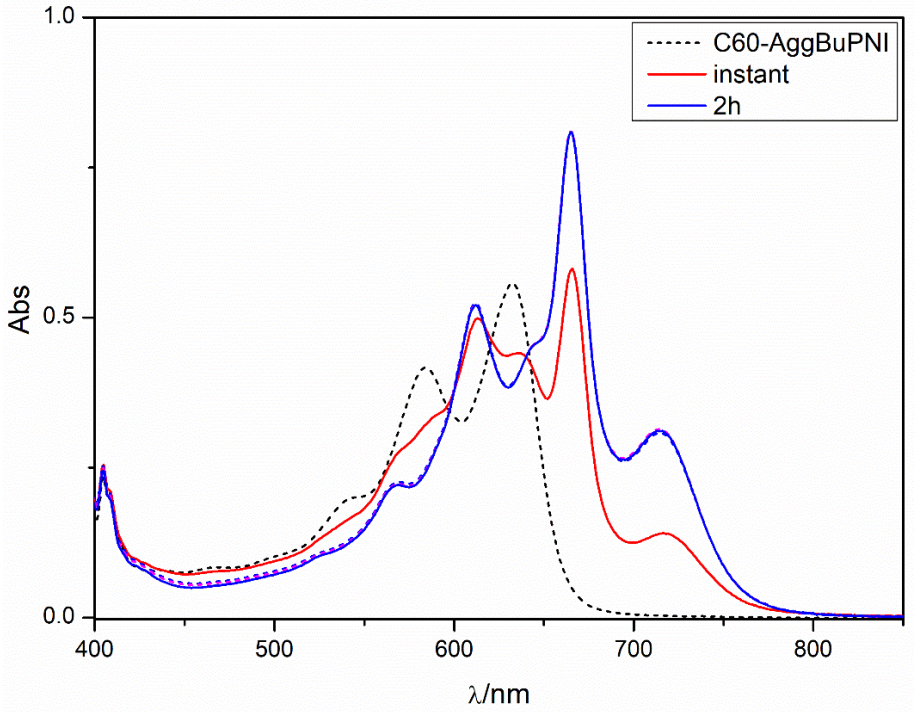

Figure S32. Spectral changes during dis-assembly of C60-**Agg**$^{\mathbf{BuPNI}}$ and formation of TFA⊂**Agg**$^{\mathbf{BuPNI}}$ via TFA diffusion from the aqueous layer to the organic layer (95/5 v/v mixture of MCH-toluene) at a dye concentration 10 μM. The experiment was carried out by preparing a solution of C60-**Agg**$^{\mathbf{BuPNI}}$ in 95/5 v/v mixture of MCH-toluene. Immediately after placing the solution over aq. TFA solution showed the formation of TFA⊂**Agg**$^{\mathbf{BuPNI}}$ (red line, instant). The switching process completed after 2 h (blue line).

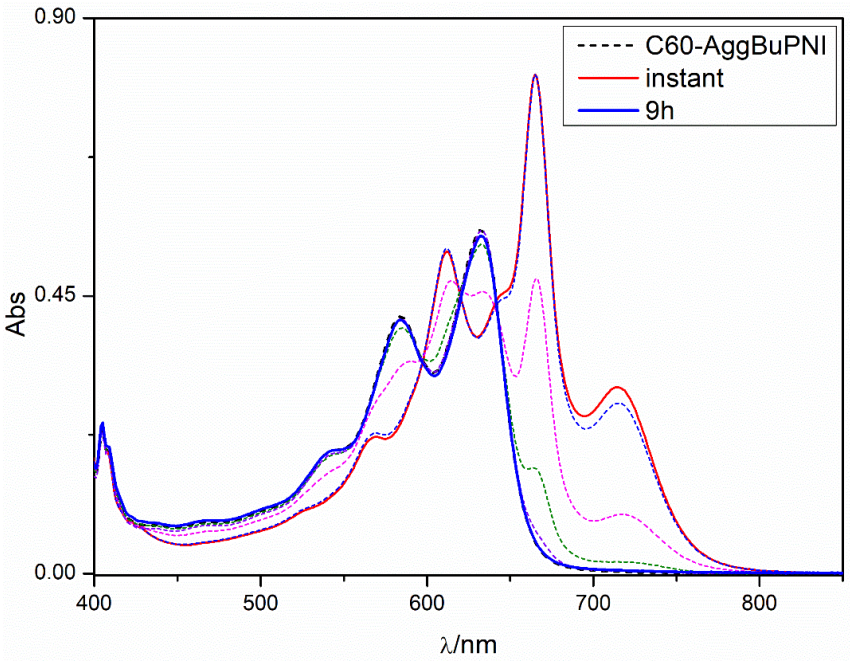

Figure S33. Spectral changes during dis-assembly of TFA⊂**Agg**$^{\mathbf{BuPNI}}$ and formation of C60-**Agg**$^{\mathbf{BuPNI}}$ via TFA diffusion from the organic (95/5 v/v mixture of MCH-toluene) layer to the aqueous layer at a dye concentration 10 μM. The aggregate TFA⊂**Agg**$^{\mathbf{BuPNI}}$ was prepared by diffusing TFA from the aqueous layer to the organic layer over a period of 2 h (previous experiment, Figure S32). The acidic-aqueous layer was then replaced with neutral water and the changes were recorded spectroscopically (dot). Generation of C60-**Agg**$^{\mathbf{BuPNI}}$ completed after 9 h (blue line). As the concentration was higher than the experiment mentioned at Figure S31, the switching process took longer period of time (9 h *vs* 6.5 h).

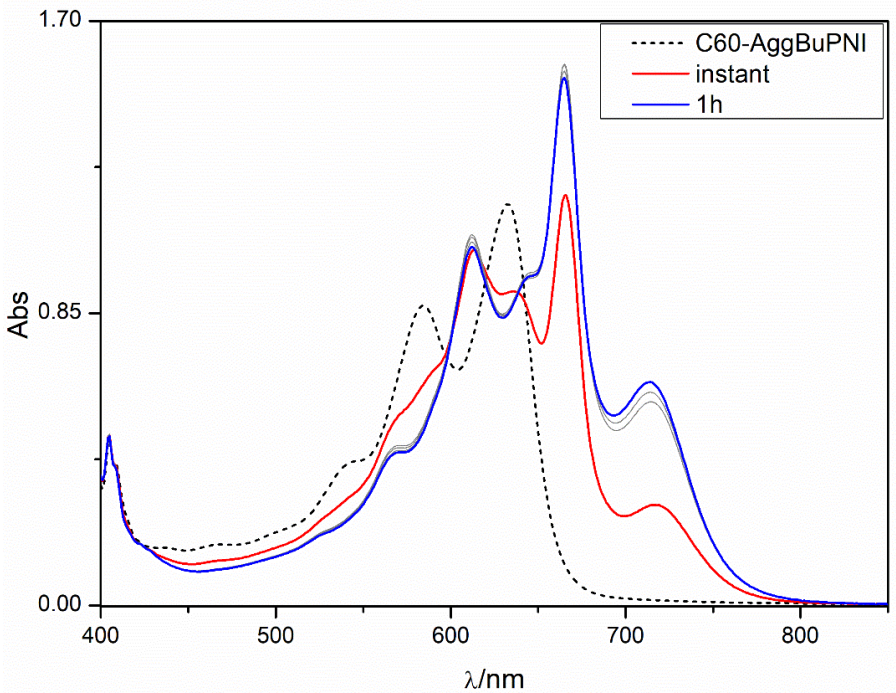

Figure S34. Spectral changes during dis-assembly of C60-**Agg**$^{\mathbf{BuPNI}}$ and formation of TFA⊂**Agg**$^{\mathbf{BuPNI}}$ via TFA diffusion from the aqueous layer to the organic layer (95/5 v/v mixture of MCH-toluene) at a dye concentration 20 μM. The experiment was carried out by preparing a solution of C60-**Agg**$^{\mathbf{BuPNI}}$ in 95/5 v/v mixture of MCH-toluene. Immediately after placing the solution over aq. TFA solution showed the formation of TFA⊂**Agg**$^{\mathbf{BuPNI}}$ (red line, instant). The switching process completed after 1 h (blue line).

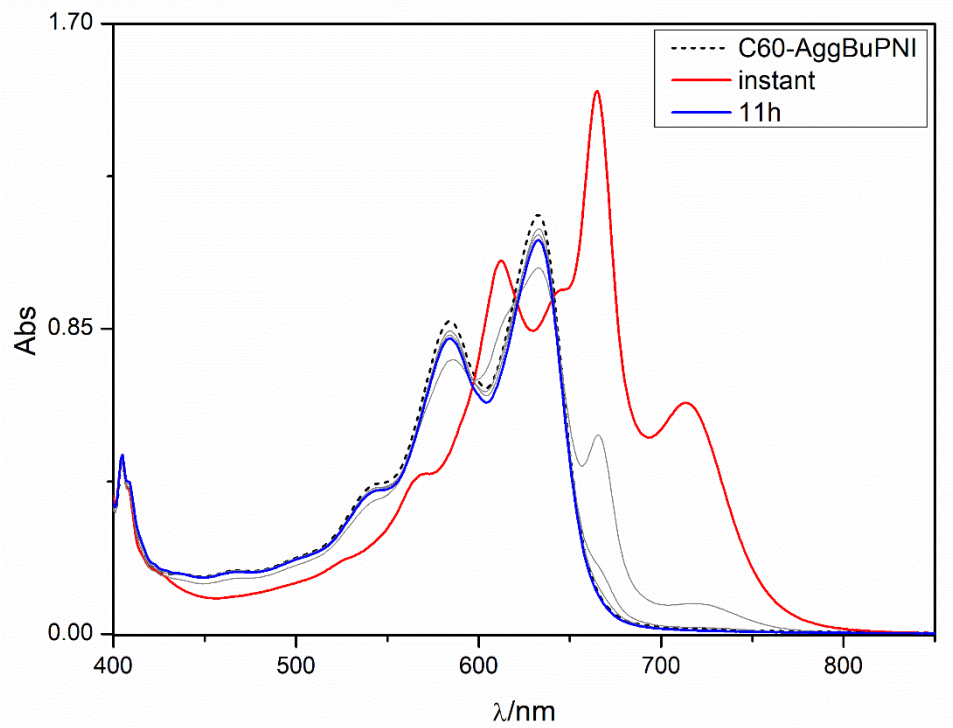

Figure S35. Spectral changes during dis-assembly of TFA⊂**Agg**$^{\mathbf{BuPNI}}$ and formation of C60-**Agg**$^{\mathbf{BuPNI}}$ via TFA diffusion from the organic (95/5 v/v mixture of MCH-toluene) layer to the aqueous layer at a dye concentration 20 μM. The aggregate TFA⊂**Agg**$^{\mathbf{BuPNI}}$ was prepared by diffusing TFA from the aqueous layer to the organic layer over a period of 1 h (previous experiment, Figure S34). The acidic-aqueous layer was then replaced with neutral water and the changes were recorded spectroscopically (dot). Generation of C60-**Agg**$^{\mathbf{BuPNI}}$ completed after 11 h (blue line). As the concentration was higher than the experiment mentioned at Figure S31, the switching process took longer period of time (11 h *vs* 6.5 h).

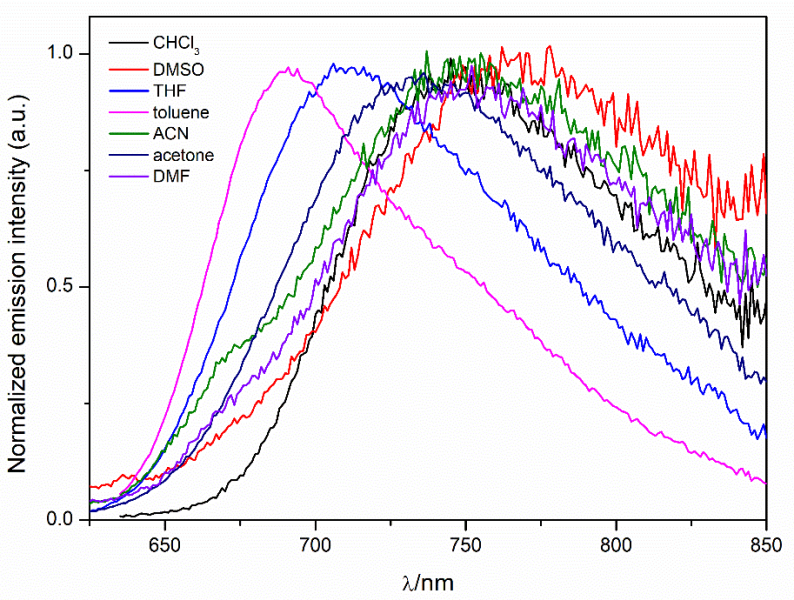

Figure S36. Photoluminescence properties of BuPNI in different solvents.

Measurement of photoluminescent quantum yields

Relative quantum yield (QY) of BuPNI was measured in $CHCl_3$, THF, toluene and MCH against using the following equation.[3]

$$\Phi^{i} = \frac{F^{i} f_{s} n_{i}^{2}}{F^{s} f_{i} n_{s}^{2}} \Phi^{s}$$

where Φ^{i} and Φ^{s} are the photoluminescence QY of the sample and that of the standard, respectively; F^{i} and F^{s} are the integrated intensities (areas) of sample and standard spectra, respectively ; *fx* is the absorption factor ($f_x = 1 - 10^{-Ax}$, where A = absorbance); the refractive indices of the sample and reference solution are n_i and n_s, respectively. The reference used was recently prepared *peri*-naphthoindigo, the quantum yield of which was determined to be 0.003 (0.3%).

Relative quantum yield of BuPNI in THF, $CHCl_3$, toluene and MCH were found to be 0.57%, 0.7 %, 1.6 % and 3.8 % respectively. With the increase in solvent polarity the chances of intramolecular hydrogen bonding decreased. As a result, the probability of rotation around the central single bond connecting the donor-acceptor pairs increased. This was reflected in the fluorescence quantum yield of the dye in different solvents. Due to more loss of fluorescence energy via rotation QY was less in polar solvents (THF and chloroform). On the other hand, the QY value was improved in the non-polar solvents (toluene and MCH) due to the restriction in intramolecular motion.

Compound	Excitation Wavelength (nm)	F_x	Absorbance	f_x	Solvent /n_x	Quantum Yield (%)
PNI	600 nm	2.59E+07	0.077325	0.16309724	THF	0.3
PNI	600 nm	2.32E+07	0.069057	0.147012	THF/	0.3
PNI	600 nm	2.16E+07	0.062558	0.134151	THF	0.3
THF						

BuPNI (1st reading)	600 nm	3.82E+07	0.060076	0.129	THF	0.56
BuPNI (2nd reading)	600 nm	4.50E+07	0.068535	0.145	THF	0.58
BuPNI (3rd reading)	600 nm	5.32E+07	0.084458	0.176	THF	0.56

Toluene						
BuPNI (1st reading)	600 nm	8.11E+07	0.049604	0.10793603	Toluene / 1.4969	1.60
BuPNI (2nd reading)	600 nm	9.31E+07	0.057387	0.12378	Toluene / 1.4969	1.62
BuPNI (3rd reading)	600 nm	1.06E+08	0.067239	0.143434	Toluene / 1.4969	1.56

MCH						
BuPNI (1st reading)	600 nm	1.50E+08	0.033585	0.074417787	MCH/1.422	3.88
BuPNI (2nd reading)	600 nm	1.75E+08	0.040874	0.0898227	MCH/1.422	3.79
BuPNI (3rd reading)	600 nm	1.99E+08	0.047476	0.103554276	MCH/1.422	3.66
$CHCl_3$						
BuPNI (1st reading)	600 nm	1.36E+07	0.087106	0.181734953	$CHCl_3$/ 1.4458	0.67
BuPNI (2nd reading)	600 nm	1.23E+07	0.084675	0.177141803	$CHCl_3$/ 1.4458	0.73
BuPNI (3rd reading)	600 nm	1.06E+07	0.063694	0.136413191	$CHCl_3$/ 1.4458	0.68

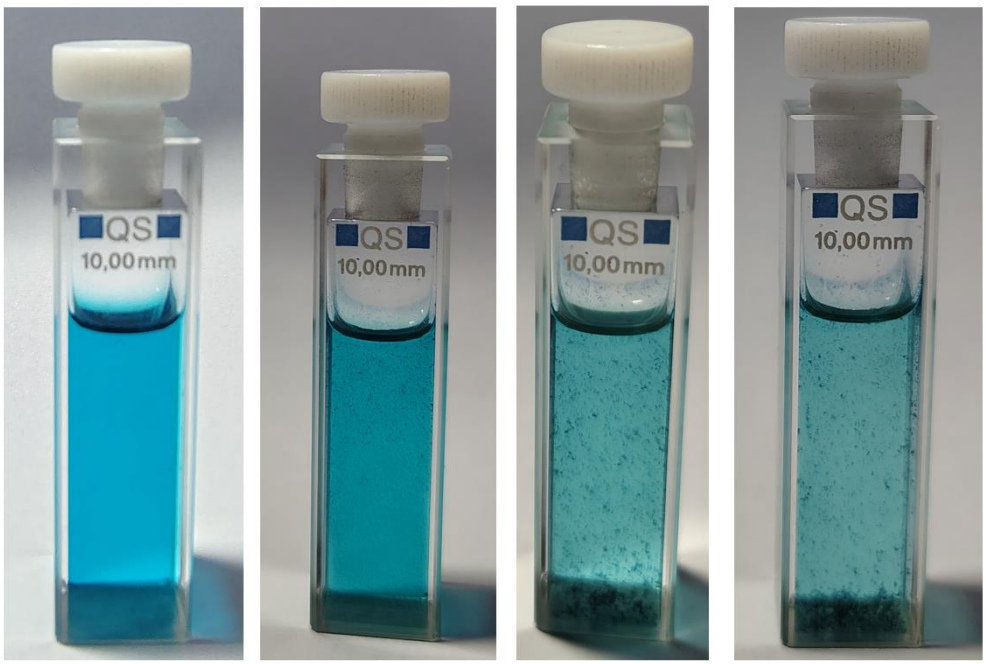

Figure S37. Visual change after addition of TFA to a solution BuPNI in MCH. Pictures were captured every 10 min after the addition.

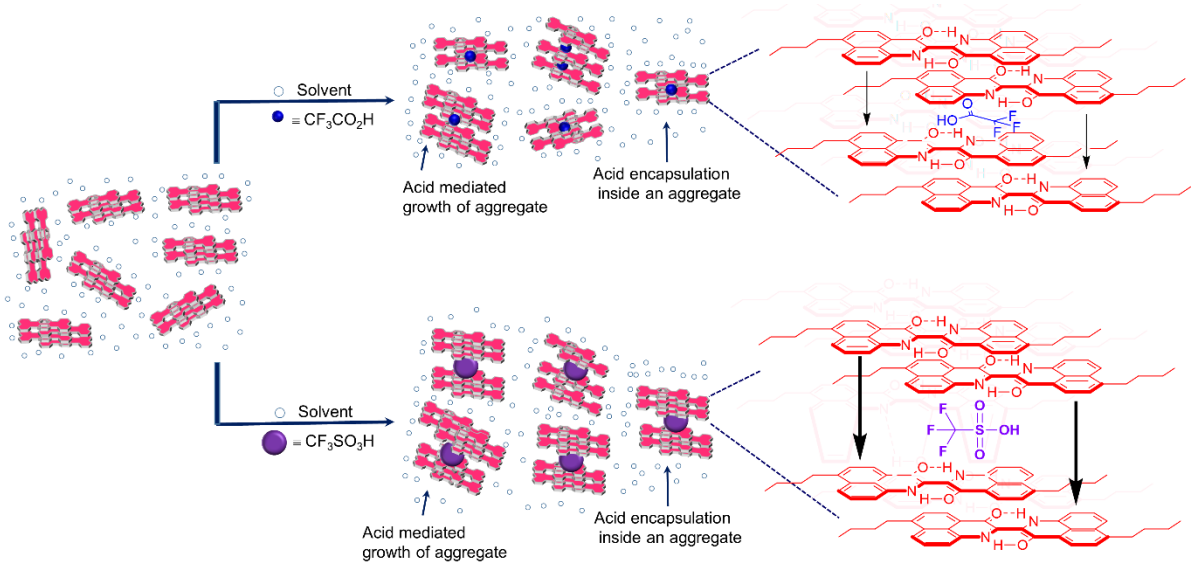

Figure S38. Differences in supramolecular rearrangement processes of **Agg^{BuPNI}** in presence of TFA and TfOH. Due to the differences in size and solvophobicity, the two guests produced different types of rearrangement. As the size of TfOH is bigger, incorporation of the same led to the fragmentation of the larger aggregates into smaller one.

6. References

1. R. J. Das. (2020). *Chemistry of peri-Naphthondigo and Analogous Compounds* [Doctoral dissertation, Indian Institute of Technology, Guwahati]. https://gyan.iitg.ac.in/handle/123456789/1876.
2. (a) M. Montazer and A. S. Maryan, Influences of Different Enzymatic Treatment on Denim Garment. *Appl Biochem Biotechnol*., 2010, **160**, 2114-2128. (b) R. Campos , A. Kandelbauer , K. H. Robra , A. Cavaco-Paulo and G. M. Gübitz , Eco-friendly TEMPO/laccase/O_2 biocatalytic system for degradation of Indigo Carmine: operative conditions and laccase inactivation, *J. Biotechnol.*, 2001, **89**, 131-139.
3. Y. Long, Y. Lu, Y. Huang, Y. Peng, Y. Lu, S.-Z. Kang and J. Mu, Effect of C_{60} on the Photocatalytic Activity of TiO_2 Nanorods, *J. Phys. Chem. C*, 2009, **113**, 13899-13905.